



What induces the spatiotemporal variability of glacier mass balance across the Qilian Mountains

Meilin Zhu^{1,2,3} · Tandong Yao^{2,5} · Lonnie G. Thompson³ · Sheng Wang⁴ · Wei Yang^{2,5} · Huabiao Zhao^{2,5,6}

Received: 20 November 2021 / Accepted: 30 March 2022 / Published online: 19 April 2022
© The Author(s), under exclusive licence to Springer-Verlag GmbH Germany, part of Springer Nature 2022

Abstract

Understanding the spatial–temporal changes in glacier mass balance and associated drivers on the Tibetan Plateau (TP) is important for predicting future water supplies and glacier-related hazards. However, the comparative study of changes in glacier mass balance in different regions of the same glacierized massif on the TP remains scarce. Combining the reconstructed detailed mass balance time-series from 1970 to 2015 for Ningchan No.1 Glacier in the eastern Qilian Mountains and Qiyi Glacier in the western Qilian Mountains using the energy and mass balance model in this work with the published mass balance data from different glaciers, we find that interannual changes in glacier mass balance are broadly similar in different regions of the Qilian Mountains. These interannual changes are primarily driven by variations in ablation-season (June–September) air temperature (T_a), which impact albedo and melt by changing snowfall and incoming longwave radiation (L_{in}). We link such interannual mass balance variability to the combination of changes in atmospheric circulation over Europe and changes in sea surface temperature (SST) in the Northwest Pacific during the ablation season which can cause the changes in T_a across the Qilian Mountains. In addition, we find a trend of increasingly negative glacier mass balance across the Qilian Mountains from 1970–1994 compared to 1995–2015. This interdecadal trend is driven by higher ablation-season T_a through increasing L_{in} and through increasing precipitation falling as rain. Lastly, higher glacier mass loss in the east than in the west Qilian Mountains from 1970–1994 and 1995–2015 was mainly caused by lower glacier area-altitude distribution, as well as a reduction in ablation-season precipitation in the eastern Qilian Mountains.

Keywords Glacier mass balance · Climate change · Atmospheric circulation · Qilian Mountains · Sea surface temperature

1 Introduction

The Tibetan Plateau and its surrounding areas contain the largest number of glaciers apart from polar regions (Yao et al. 2012). These glaciers can provide detailed paleoclimatic information in the subtropics (Aizen et al. 2004; Thompson et al. 1989; Yao et al. 2006) and their melt-water runoff feeds some important rivers (such as Indus, Amu Darya, Ganges–Brahmaputra, and Tarim) on the Asia (Armstrong et al. 2019; Immerzeel et al. 2020; Gao et al. 2021; Pritchard 2019). The recent studies indicated that on the interdecadal timescales during the past several decades, glacier mass balances on the TP have undergone different changes: glaciers in the eastern Pamir, Karakoram, and western Kunlun regions have exhibited slight mass stability or even glacier advance, while most of the glaciers have had an accelerated shrinkage and mass loss (Azam and Srivastava 2020; Brun et al. 2017; Barandun et al. 2015; Farinotti et al. 2020; Fujita and Nuimura 2011; Käab et al. 2015; Kumar

✉ Meilin Zhu
meilin.zhu@itpcas.ac.cn

✉ Lonnie G. Thompson
thompson.3@osu.edu

- ¹ Center for the Pan-Third Pole Environment, Lanzhou University, Lanzhou 730000, China
- ² Key Laboratory of Tibetan Environment Changes and Land Surface Processes, Institute of Tibetan Plateau Research, Chinese Academy of Sciences (CAS), Beijing 100101, China
- ³ Byrd Polar and Climate Research Center, The Ohio State University, Columbus 43210, OH, USA
- ⁴ Geography Science Institute, Shanxi Normal University, Linfen 041081, China
- ⁵ CAS Center for Excellence in Tibetan Plateau Earth Sciences, Beijing 100101, China
- ⁶ Ngari Station for Desert Environment Observation and Research, Institute of Tibetan Plateau Research, CAS, Tibet, China

et al. 2019; Pan et al. 2012; Shean et al. 2020; Wang et al. 2010, 2017; Yang et al. 2016; Yao et al. 2012; Zemp et al. 2019; Zhou et al. 2018; Zhang et al. 2012, 2021; Zhu et al. 2018b, 2021b). And some glaciers could almost disappear in some mountain ranges in this century (Zemp et al. 2019). These changes are believed to have a profound influence on the future vulnerability of water resources, glacier-related hazards, surrounding environments, and downstream social and economic development (Immerzeel et al. 2020; Kääb et al. 2018; Marzeion et al. 2014; Nie et al. 2021; Radić et al. 2014; Thompson 2000; Yao et al. 2019; Zhang et al. 2016). Thus, understanding the climatic factors that drive the spatial–temporal changes in glacier mass balance on the TP is important.

Recent studies show that the rates of glacier mass loss on the southern, central, and northeastern TP, and the western Himalayas increased over the last several decades (Azam and Srivastava 2020; Kumar et al. 2019; Wang et al. 2010; Yao et al. 2012; Yang et al. 2016; Zhang et al. 2012). A variety of factors have been proposed to explain this phenomenon, including increased light-absorbing particles (such as black carbon), expanded proglacial lake, and reduced precipitation (Chen et al. 2020; Kang et al. 2020; Maurer et al. 2019; Yao et al. 2012). However, most studies thought that regional warming is the main reason for the increasing rates of glacier mass loss over the last several decades (Azam and Srivastava 2020; Bhattacharya et al. 2021; Chen et al. 2020; Sun et al. 2018a; Yang et al. 2016; Zhang et al. 2012, 2021; Zhu et al. 2021a). Increased air temperature (T_a) reduces snowfall by increasing the precipitation falling as rain, which can decrease accumulation and albedo (Kumar et al. 2019; Oerlemans 2001; Favier et al. 2004a; Zhu et al. 2018a). Thus, increased T_a leads to enhanced mass loss by increasing melt and reducing accumulation. In addition, T_a information is transferred to the glacier surface mainly through incoming longwave radiation (L_{in}), which is also an important heat source for melt (Ohmura 2001). However, the importance of L_{in} for the interannual and interdecadal changes in mass balance for those glaciers has not been discerned due to the lack of long-term energy and mass balance data. Some studies found that L_{in} plays an important role in the seasonal changes of the melt energy for the glaciers through changing clouds and humidity (Sicart et al. 2005; Yang et al. 2011) and in the spatial distribution of melt energy of glaciers in different regions of the TP due to different climate backgrounds (Zhu et al. 2018a).

In addition, increased knowledge of the spatial distribution of interdecadal changes in glacier mass balance for the same periods among different regions on the TP has been gained (Brun et al. 2017; Bhattacharya et al. 2021; Shean et al. 2020; Zhu et al. 2018a, 2021a; Zhou et al. 2018), however, the comparative study of changes in glacier mass balance in different regions of the same glacierized massif on

the TP remain scarce, especially for interannual timescales. Maurer et al. (2019) analyzed the interdecadal changes in mass balance in different regions of the Himalayas. Most studies have applied the glacier model to study interannual changes in glacier mass and their drivers on the TP (Cao et al. 2019; Chen et al. 2020; Mölg et al. 2014; Wang et al. 2010; Wang et al. 2017; Yang et al. 2016; Zhang et al. 2021; Zhu et al. 2018b, 2021b) but mainly focused on a single glacier or set of glaciers within the same region with similar climate changes. For example, Zhang et al. (2021) found that the July East-Atlantic index was highly correlated with the cumulative positive temperature and inversely related to the reconstructed mass balance of Shiyi Glacier in the central Qilian Mountains using a degree-day model through a zonal atmospheric teleconnection pattern. The question is whether these conclusions from one glacier can be used to explain the interannual/interdecadal changes in glacier mass balance across the Qilian Mountains or just in the central Qilian Mountains. Comparison of glacier mass balance changes in different regions can improve our understanding of coordinated variations of glacier mass balance and associated regional climate variables and macro-scale atmospheric circulation (Favier et al. 2004a, b).

The Qilian Mountains in the northeastern TP host 2684 individual glaciers (Sun et al. 2018a, b). The climates in Qilian Mountains are mainly influenced by the mid-latitude westerlies and East Asian monsoon, and the strengths of these circulations are different between the eastern and western Qilian Mountains (Wang et al. 2010; Yao et al. 2012, 2013). Those glaciers are rapidly retreating across all regions (Neckel et al. 2014; Pan et al. 2012; Shean et al. 2020; Sun et al. 2018a; Yao et al. 2012) but are doing so much faster in the eastern Qilian Mountains compared to the central-western region (He et al. 2019; Sun et al. 2018a). It is a good site to carry out the study of spatial–temporal changes in glacier mass balance on the TP, because four glaciers across the Qilian Mountains have established glaciological monitoring campaigns and some meteorological stations along the Qilian Mountains provide the long time series of meteorological data. Qiyi Glacier has been observed for more than 20 years since 1974 although the data is inconspicuous. It is the longest mass balance data on the TP except for Xiaodongkemadi Glacier in the central TP (Yao et al. 2012). Three other glaciers are observed since 2010 or later (Cao et al. 2017; Liu 2018; Zhang et al. 2021). These provided available databases to drive the energy and mass balance (EMB) model which describes the detailed physical processes of glacier accumulation and ablation (Ding et al. 2017; Fujita and Nuimura 2011; Guo et al. 2021; Hock and Holmgren 2005; Jiang et al. 2010; Liu et al. 2021; Reijmer and Hock 2008; Sun et al. 2018b; Zhu et al. 2020). This method has been used to reconstruct worldwide long-term glacier mass balance (Anderson and Mackintosh 2012; Bonekamp et al.

2019; Fujita and Nuimura 2011; Mattea et al. 2021; Möller et al. 2016; Mölg et al. 2014; Van Pelt et al. 2019; Vandecrux et al. 2021; Yang et al. 2016; Zhu et al. 2018b, 2021b). And these results are reasonable and very useful to quantify the spatial–temporal changes in glacier mass balance and melt-water and their climate drivers. The objectives of this study are: (1) to reconstruct mass balance records of Qiyi Glacier in the west and Ningchan No.1 Glacier in the eastern Qilian Mountains from 1970 to 2015 using an EMB model, (2) to investigate the spatiotemporal patterns of glacier mass balance across the Qilian Mountains by comparing these two reconstructed mass balance datasets and the other published mass balance datasets, and (3) to analyze the relationships between glacier mass balance and regional climate regimes, and provide insights into the atmospheric circulation that is responsible for the interannual/interdecadal changes in glacier mass balance across the Qilian Mountains. This research has practical implications for understanding the spatial–temporal changes of glacier mass balance and improving our ability to reconstruct and predict water availability in the arid and semi-arid regions around the Qilian Mountains and on the Tibetan Plateau.

2 Study area, method and data

2.1 Study area

Our study glaciers (Fig. 1), Qiyi Glacier (39° 14' 20.94" N, 97° 45' 25.72" E) and Ningchan No.1 Glacier (37° 30' 47.60" N, 101° 50' 18.73" E), are typical sub-continental (Shi and Liu 2000), valley-type glaciers largely free of supraglacial debris cover (Fig. S1 in the Supplementary Material). Qiyi Glacier is located on the north slope of the Tuolai Mountains (Fig. 1a) and can be treated as a typical glacier of the western Qilian Mountains. The glacier flows northward from an elevation of 5159 to 4304 m a.s.l. and has an area of approximately 2.87 km² (Yao et al. 2012), with the median elevation (where elevation divides glacier area equally) of 4780 am a.s.l. in 2000 (Fig. 1b). Records from Tuole station, which is located approximately 70 km from Qiyi Glacier (Fig. 1a), show that 92% of the annual precipitation occurs between May and September (Fig. 1d). Ningchan No.1 Glacier had an area of approximately 0.39 ± 0.04 km² in 2014 (Cao et al. 2017) and is located on the northern slope of the Lenglongling Mountains, eastern

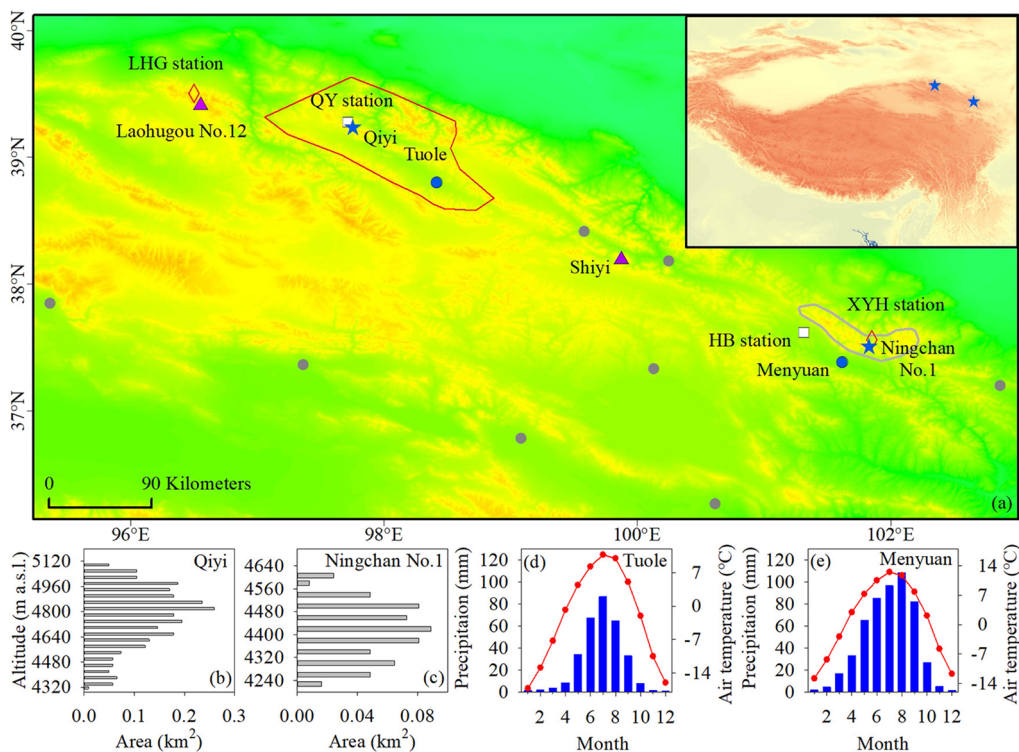


Fig. 1 Locations of Qiyi and Ningchan No.1 glaciers (blue stars), Shiyi and Laohugou No.12 glaciers (pink triangles), the Beida River region (red line), the Lenglongling Mountains (grey line), Tuole and Menyuan station (blue points) in the Qilian Mountains; Laohugou (LHG) and Xiyinghe (XYH) stations (red diamonds), Haibei (HB) and Qiyi (QY) stations (white squares), as well as eight other meteorological stations (grey points) with an altitude higher than 2500 m

a.s.l. (a). The area-altitude distribution of Qiyi Glacier (b) and Ningchan No.1 Glacier (c) based on glacier boundaries in 2000 and the Shuttle Radar Topography Mission digital elevation model. Mean monthly air temperature (red dotted line) and precipitation (blue histogram) at Tuole station (d) and Menyuan station (e) during 1970–2015

Qilian Mountains (Fig. 1a). Its altitudinal range is from 4260 to 4640 m a.s.l. (Cao et al. 2017), with the median elevation of about 4400 m a.s.l. in 2000 (Fig. 1c). Meteorological records from Menyuan station, which is located approximately 25 km from Ningchan No.1 Glacier (Fig. 1a), show 83% of the annual precipitation occurs from May to September (Fig. 1e). The westerlies dominate the regional climate of the western Qilian Mountains (Yao et al. 2012), whereas the eastern Qilian Mountains are dominated by westerlies and the Asian summer monsoon (Yang et al. 2014; Li et al. 2015).

2.2 The energy and mass balance model and input data

We apply an EMB model in this study which is fully described in Fujita and Ageta (2000) and Yang et al. (2013). Here we mainly present the most important features of the model. The model solves the following equations:

$$Q_M = S_{in}(1 - \alpha) + L_{in} + L_{out} + H_{sen} + H_{lat} + QG \quad (1)$$

$$M = \int \left(\frac{Q_M}{L_m} + \frac{H_{lat}}{L_v} + C_{en} + P_{snow} \right) dt \quad (2)$$

where Q_M is the melt energy, S_{in} is the incoming shortwave radiation, α is the surface albedo, L_{in} is the incoming longwave radiation, L_{out} is the outgoing longwave radiation, H_{sen} is the sensible heat flux, and H_{lat} is the latent heat flux. QG is the subsurface heat flux, which consists of conductive heat flux (G) and an energy flux due to penetrating shortwave radiation (QPS). Q_M is defined as positive when it is larger than 0, and other fluxes are defined as positive when they are directed towards the surface. The point mass balance (M) is composed of melt, sublimation/evaporation, refreezing (C_{en}) and solid precipitation (P_{snow}). And meltwater is the absolute value of the melt. L_m is the latent heat of ice melt and L_v is the latent heat of evaporation/sublimation. Differing from the previous version (Yang et al. 2013), we include new features based on published work: (i) albedo is incorporated following Oerlemans and Knap (1998); (ii) L_{in} is calculated using the clear-sky parameterization of Brunt (1932) combined with a cloud correction described by Crawford and Duchon (1999).

$$L_{in} = \sigma(T_a + 273.15)^4((1 - \tau_{atm}) + \tau_{atm} * (b_1 + b_2(\sqrt{e_a}))) \quad (3)$$

where σ is the Stefan-Boltzmann constant ($5.67 \times 10^{-8} \text{ W m}^{-2} \text{ K}^{-4}$); T_a is the air temperature at the height of 2 m ($^{\circ}\text{C}$); τ_{atm} is the ratio of the measured S_{in} to the solar radiation at the top of the atmosphere; e_a is the vapor pressure (hPa) calculated from relative humidity and air temperature. For Qiyi and Ningchan No.1 glaciers, the two

constants (b_1 and b_2) of the L_{in} model were optimized using the measured L_{in} , air temperature, and relative humidity at Laohugou station (Qin 2018; Sun et al. 2011) and Xiyinghe station (XYH, Zhao and Zhang 2019) (Fig. 1a), respectively. The modelled L_{in} agreed well with the measured values at the two sites (Fig. S2). Laohugou station and Xiyinghe station are located about 110 km northwest of Qiyi Glacier and about 5 km northeast of Ningchan No.1 Glacier, respectively. A detailed description of the EMB model used in this study along with its parameters are presented in Text S1 and Table S1 in the Supplementary Material, respectively.

Meteorological data from Tuole station and Menyuan station are used to force the EMB model over a period of 46 years from October 1969 to September 2015 at 40 m vertical intervals and a daily time-step for Qiyi and Ningchan No.1 glaciers, respectively. Time series of daily mean air temperature (T_a), daily mean relative humidity (RH) and daily precipitation are interpolated to each elevation band using their vertical gradients. Hoffman et al. (2008) found that the daily time-step EMB model can be used to model the ablation process that likely occurs over shorter time-scales, and monthly and seasonal totals of ablation seem robust for the daily time-scale EMB model. The comparison of measured discharge and mass balance and modelled values from the daily time-scale EMB model (Fujita and Sakai 2014; Yang et al. 2016; Zhang et al. 2012) also support the point of Hoffman et al. (2008). However, some parameters of the energy and mass balance model are different between the hourly and daily time-scale EMB model (Hoffman et al. 2014), which means that the calibrated parameters for the hourly time-scale EMB model need to modify when we use these parameters in the daily time-scale EMB model. In this work, we mainly analyze the seasonal totals of mass balance components, thus, the daily time-scale EMB model is suitable.

Daily mean wind speed (WS) for each glacier is assumed to be independent of the altitude, because the WS data on the glacier is considered too sparse to derive a general scheme to quantitatively assess the spatial distribution of wind speed (Hock and Holmgren 2005). The gradients in precipitation and T_a for each glacier are obtained from the measured meteorological data at different altitudes around the glacier (Cao et al. 2019; Wang et al. 2009). Daily mean S_{in} at Tuole and Menyuan stations are estimated from their respective sunshine duration, RH , T_a , air pressure and their geographic location (latitude, longitude and altitude) (Yang et al. 2001). Modelled S_{in} at Tuole and Menyuan stations were corrected by measured S_{in} at 4295 m a.s.l. near Qiyi Glacier over the period 2002–2005 (Fig. 1a, Sakai et al. 2006) and at Haibei station (Fig. 1a, Zhu and Peng 2019) near Ningchan No.1 Glacier from 2014 to 2015, respectively. The detailed information about daily mean S_{in} can be seen in Text S1. The

corrected S_{in} for each glacier is assumed to be independent of the altitude. All parameters are presented in Table S1.

Temporal changes in glacier area are considered in the model using the different boundaries of each glacier over different years. For both glaciers, glacier boundaries between 1970 and 1994 were taken from Landsat TM image from 1990; and between 1995 and 2009 were taken from Landsat TM image from 2000. Glacier outlines were digitized on-screen manually from the Landsat image, depending on false colour image composites (TM: RGB by bands 543) (Ye et al. 2017). The uncertainty of glacier boundaries obtained by this method is always below the mapped glacier area of 6% (Bolch et al. 2010; Shangguan et al. 2014; Ye et al. 2017). And glacier boundaries between 2010 and 2015 are represented by the boundary in 2015 from Li et al. (2019a). The area distribution at each elevation band (hypsometry) of these glaciers is derived from these glacier boundaries and the 90 m Shuttle Radar Topography Mission digital elevation model (<https://glervis.usgs.gov/>). In this study, only parameter values required by the albedo model were tuned to achieve the best match between the modelled and in-situ mass balance (including the annual glacier-wide mass balance and point mass balance). First, the model was adjusted to minimize the root mean square error (RMSE) between measured and modelled annual glacier-wide mass balance, taking advantage of long-term mass balance observations on Qiyi Glacier. Second, the model was retuned until the resulting RMSE between the measured and modelled point mass balance was minimized. Meanwhile, the RMSE between measured and best modelled annual glacier-wide mass balance is between 90 and 110% of the minimum RMSE in the first model iteration. For Qiyi Glacier, the measured mass balances from 2005/06 balance year to 2014/15 balance year were used for calibrating the parameters in the model, and measured mass balances during 1970–2004, modelled mass balance from Wang et al. (2017) and periodic geodetic mass balance data from Shean et al. (2020) were used for validating the simulated results. For Ningchan No.1 Glacier, the measured mass balances from 2010/11 balance year to 2014/15 balance year were used for calibrating the parameters in the model, and the modelled regional mass balance data in the Lenglongling Mountains from Cao et al. (2019) and the geodetic mass balance data from Shean et al. (2020) were used for validating the simulated results.

2.3 Other data

Monthly air temperature and precipitation records from 10 Chinese national meteorological stations near the Qilian Mountains at elevations above 2500 m (Fig. 1) are used to analyze the spatial correlations between glacier mass balance and regional climate variables. Additionally, to investigate glacier mass changes from a macroscale atmospheric

circulation perspective, the following data products are utilized in the present investigation: the monthly geopotential height and wind fields at 500 hPa from the Japanese 55-year reanalysis dataset (JRA55, $1.25^\circ \times 1.25^\circ$, 1958–2019) (Kobayashi et al. 2015), the monthly sea surface temperature (SST) from the Hadley Centre Sea Ice and Sea Surface Temperature dataset (HadISST) ($1^\circ \times 1^\circ$, Rayner et al. 2003), and monthly gridded air temperature data and precipitation data from CN05.1 which is based on interpolation from over 2400 daily station reports in China ($0.25^\circ \times 0.25^\circ$, Wu and Gao 2013; Xu et al. 2009). Lastly, to investigate glacier mass changes in the Qilian Mountains from a regional perspective, the reconstructed annual mass balances for Laohugou No.12 Glacier in the western Qilian Mountains (Chen et al. 2020) and for Shiyi Glacier in the central Qilian Mountains (Zhang et al. 2021), and the reconstructed regionally-averaged annual mass balance for 631 glaciers (total area of 318.2 km²) in the Beida River catchment ($97^\circ \sim 99.5^\circ$ E, $38^\circ \sim 40^\circ$ N) in the western Qilian Mountains (Wang et al. 2017) and for 244 glaciers (103.2 km²) in the Lenglongling Mountains ($101.2^\circ \sim 102.5^\circ$ E, $37.3^\circ \sim 37.9^\circ$ N) in the eastern Qilian Mountains (Cao et al. 2019) are also used in this work (Fig. 1). These mass balances are modelled using the degree-day model and meteorological data from different stations, and calibrated by measured mass balance and/or periodic geodetic mass balance data.

3 Results

3.1 Model calibration, validation and uncertainty analysis

For Qiyi Glacier, the modelled mass balance for different years largely agreed with the available in-situ mass balance observation taken at different altitudes (Fig. 2; Pu et al. 2005; Wang et al. 2017; Yao et al. 2012). The RMSE between measured and modelled point mass balance at all stakes is 333 mm w.e. for the seven years presented in Fig. 2. The simulations of annual glacier-wide mass balance are in good accord with observations (correlation coefficient, $r=0.92$, $p<0.01$, $n=20$ and $RMSE=162$ mm w.e., Fig. 3); the simulated and observed multi-year averaged glacier-wide mass balances were -208 and -248 mm w.e. a^{-1} , respectively. The correlation coefficients used in this study are obtained using the Pearson correlation analysis. In addition, the simulated glacier-wide mass balance of Qiyi Glacier in this study shows a good agreement with Wang et al. (2017) ($r=0.89$ and $RMSE=139$ mm w.e. a^{-1} ; Fig. 3a). The average glacier-wide mass balance over 1970–2013 was -214 mm w.e. a^{-1} , which is only 10 mm w.e. a^{-1} larger than the value determined by Wang et al. (2017).

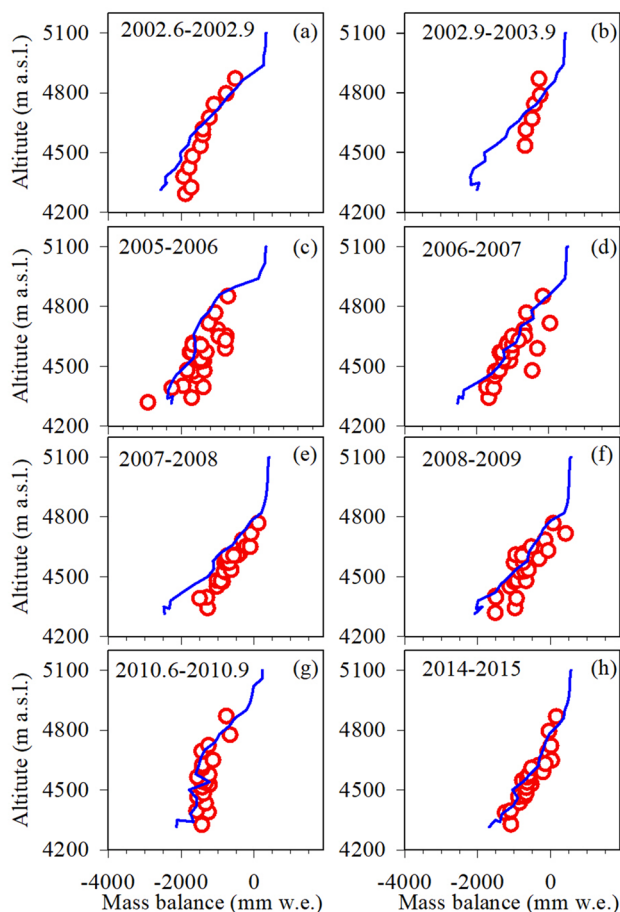


Fig. 2 Comparison of modelled (blue line) and measured (red circles) mass balance as a function of elevation in different years (a–g), and modelled and measured glacier-wide mass balance for different years (h) on Qiyi Glacier

The simulated mass balance corresponds well with the in-situ mass balance observations at different altitudes and on a glacier-wide basis on Ningchan No.1 Glacier (Fig. 4; Cao et al. 2017). The RMSE between measured and modelled point mass balance at all stakes is 352 mm w.e. for the five years presented in Fig. 4. The modelled mean glacier-wide annual mass balance from 2010/11 to 2014/15 was approximately -971 mm w.e. a^{-1} , which corresponds well with the measured value of -900 mm w.e. a^{-1} . Glacier mass balance from the degree-day model for the Lenglongling Mountains (Fig. 1) during 1972–2015 (Cao et al. 2019) also agrees with our reconstructed mass balance for Ningchan No.1 Glacier ($r=0.9$, $p<0.01$). In addition, Shean et al. (2020) estimated an average mass balance of -233 ± 93 mm w.e. a^{-1} for Qiyi Glacier and -478 ± 350 mm w.e. a^{-1} for Ningchan No.1 Glacier between 2000 and 2018. The measured mean glacier-wide mass balance for Qiyi Glacier was -480 mm w.e. a^{-1}

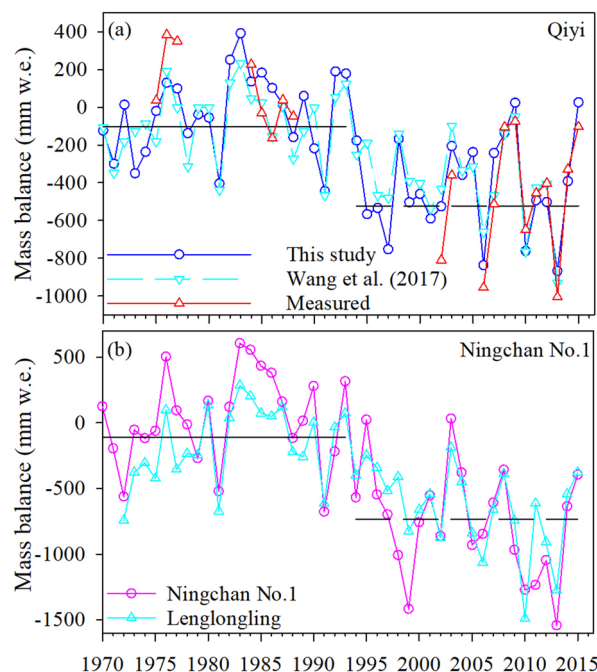


Fig. 3 **a** Comparison between the modelled and measured annual mass balance for Qiyi Glacier, with respect to the reconstructed mass balance of Qiyi Glacier from Wang et al. (2017); **b** comparison between the modelled mass balance on Ningchan No.1 Glacier and the reconstructed regionally-averaged glacier annual mass balance of the Lenglongling Mountains (Cao et al. 2019). The black line and black dashed line represent the average mass balance of both glaciers during 1970–1994 and 1995–2015 in this study, respectively

during 2002–2015. Our modelled values (-400 ± 149 mm w.e. for Qiyi Glacier and -773 ± 286 mm w.e. for Ningchan No.1 Glacier) for 2000–2015 lie within the uncertainties of the values presented in Shean et al. (2020). These results confirm that the EMB model satisfactorily reconstructs the mass balance variations from 1970 to 2015 for Qiyi and Ningchan No.1 glaciers.

The uncertainties in modelled glacier-wide mass balances originate mainly from parameters in the albedo model which are unknown in this work. To determine uncertainties for these parameters and their impact on results, they were perturbed by $\pm 10\%$ from their original/calibrated values (Table S2) and the model was run again. This is a common method in the model to estimate the uncertainty when parameters are unknown (Azam and Srivastava 2020; Zhu et al. 2021a). The total uncertainty in the modelled annual glacier-wide mass balance was estimated by adding all the parametric uncertainties, using error propagation theory, to yield a total uncertainty of ± 149 and ± 286 mm w.e. a^{-1} for modelled glacier-wide mass balance on Qiyi and Ningchan No.1 glaciers, respectively.

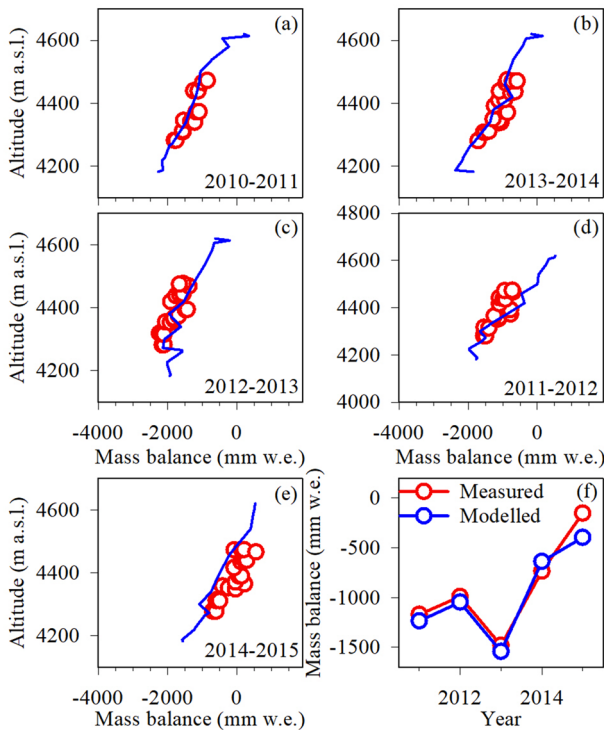


Fig. 4 Comparison of modelled (blue line) and measured (red circles) mass balance as a function of elevation in different years (a–e), and modelled and measured glacier-wide mass balance in different years (f) on Ningchan No.1 Glacier

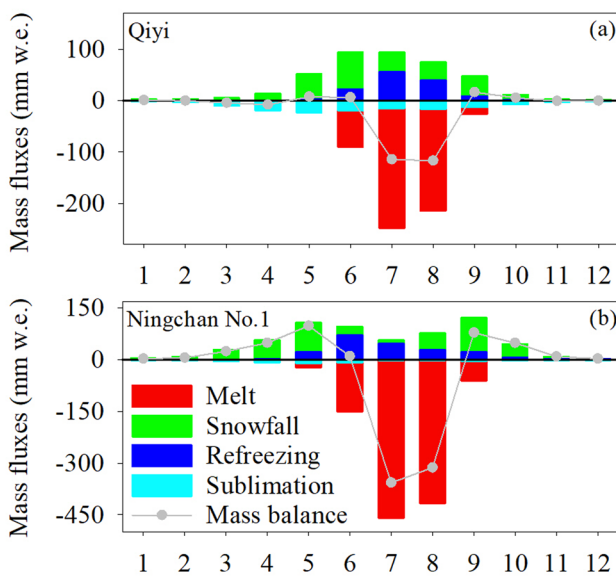


Fig. 5 Average monthly mass fluxes of the mass balance components on a Qiyi and b Ningchan No.1 glaciers during 1970–2015

3.2 Seasonal cycle in glacier mass balance components

Annual melt is the largest mass balance component at the two glaciers. Melt predominantly occurs during the ablation season and the mean monthly melt is significantly stronger in July–August than in other months on both glaciers (Fig. 5). The absolute value of mean ablation-season melt is about 1.9 times larger on Ningchan No.1 Glacier than on Qiyi Glacier (Table 1 and Fig. 5). The main source of mass accumulation at the two glaciers is snowfall (Table 1). Most snowfall occurs in May–September on Qiyi Glacier and in March–October on Ningchan No.1 Glacier (Fig. 5). Snowfall is 220 mm w.e. a⁻¹ larger in the ablation season than in the cold season (October–May) on Qiyi Glacier, while snowfall is only 90 mm w.e. a⁻¹ less in the ablation season than in the cold season on Ningchan No.1 Glacier. This indicates that the character of seasonal snowfall is slightly different at the two glaciers, even though this precipitation mainly occurs during the ablation season. This indicates a higher influence of T_a on snowfall during the ablation season for Ningchan No.1 Glacier than Qiyi Glacier. 18% and 45% of ablation-season glacier-wide precipitation falls on glacier surface as rain on Qiyi and Ningchan No.1 glaciers, respectively (Table 1). Mean annual snowfall is 214 mm w.e. a⁻¹ higher on Ningchan No.1 Glacier than Qiyi Glacier (Table 1) mainly due to higher snowfall in March–May and October on Ningchan No.1 Glacier (Fig. 5). Such high snowfall contributes to lower ice area–elevation distribution on Ningchan No.1 Glacier than Qiyi Glacier (Fig. 1). Refreezing and sublimation/evaporation are quite small (Table 1 and Fig. 5). Refreezing largely occurs in the ablation season when strong melt occurs (Fig. 5). And refreezing was slightly higher on Ningchan No.1 Glacier than on Qiyi Glacier in different seasons (Table 1). Sublimation/evaporation occurs year-round, and it was slightly higher on Qiyi Glacier than on Ningchan No.1 Glacier in different seasons (Table 1). Except for July and August, the mean monthly mass balance is close to zero for Qiyi Glacier because of the small ablation and snowfall accumulation (Fig. 5a). For Ningchan No.1 Glacier, the mean monthly mass balance is significantly positive during March–May and September–October due to the reduced ablation and high snowfall accumulation (Fig. 5b). Significant and most mass loss is found in July and August due to strong melt, which causes the negative mass balance on both glaciers (Fig. 5). The mean annual mass balance is -211 ± 149 and -340 ± 286 mm w.e. a⁻¹ on Qiyi and Ningchan No.1 glaciers (Table 1), respectively.

Table 1 The seasonal meteorological variable at stations and seasonal glacier-wide mass balance components for Qiyi and Ningchan No.1 glaciers during 1970–2015

Scale	Variable	Qiyi			Ningchan No.1		
		Cold	Ablation	Annual	Cold	Ablation	Annual
Station	Precipitation (mm)	59	251	310	156	372	528
	T_a (°C)	-7.8	8.5	-2.4	-3.6	10.6	1.1
Glacier-wide (mm w.e. a ⁻¹)	Mass balance	-1 (48)	-210 (242)	-211 (267)	241 (51)	-582 (399)	-340 (413)
	Snowfall	89 (28)	309 (64)	398 (74)	261 (48)	351 (81)	612 (92)
	Refreezing	4 (3)	125 (31)	129 (31)	34 (17)	168 (24)	203 (24)
	Sublimation	-69 (12)	-64 (11)	-133 (18)	-30 (6)	-16 (5)	-46 (8)
	Melt	-25 (18)	-580 (207)	-605 (216)	-24 (15)	-1085 (326)	-1109 (326)
	Rain	0	69	69	4	282	285
	Precipitation	89	378	467	265	633	897

The values in the bracket are standard deviations of the detrending variables

3.3 Interannual variability in glacier mass balance components

The magnitudes of interannual variations (or standard deviations) in each cold-season mass balance component

are significantly smaller than those in each ablation-season value (Table 1), indicating that interannual mass balance variability mainly occurs in the ablation season. The standard deviation of ablation-season melt and snowfall is significantly larger than that of ablation-season refrozen water and

Fig. 6 Seasonal mass fluxes of the mass balance components on **a** Qiyi and **b** Ningchan No.1 glaciers during 1970–2015

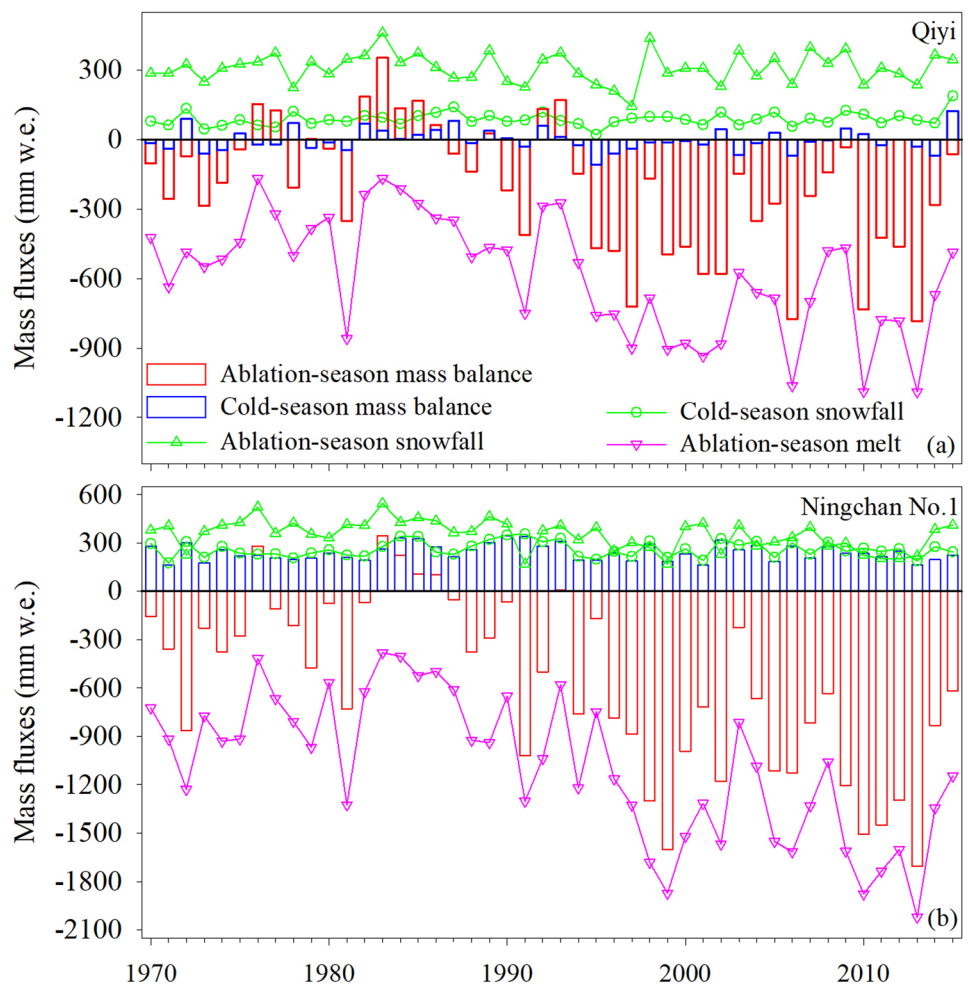


Table 2 The correlation coefficient among some variables for Qiyi and Ningchan No.1 glaciers using their detrending time series

Variables	Qiyi										Ningchan No.1									
	Ablation season					Annual					Ablation season					Annual				
	T_g at Tuole	Precipitation	Snowfall	Meltwater	Annual Precipitation	T_g at Menyuan	Precipitation	Snowfall	Meltwater	Annual Precipitation	T_g at Tuole	Precipitation	Snowfall	Meltwater	Annual Precipitation	T_g at Menyuan	Precipitation	Snowfall	Meltwater	Annual Precipitation
Annual mass balance	-0.71**	0.46**	0.75**	-0.94**	0.58**	-0.85**	0.17	0.74**	-0.98**	0.3	-0.71**	0.46**	0.75**	-0.94**	0.58**	-0.85**	0.17	0.74**	-0.98**	0.3
Annual snow	-0.37*	0.79**	0.93**	-0.63**	0.9**	-0.55**	0.47**	0.86**	-0.69**	0.66**	-0.37*	0.79**	0.93**	-0.63**	0.9**	-0.55**	0.47**	0.86**	-0.69**	0.66**
Ablation-season mass balance	-0.74**	0.48**	0.78**	-0.96**	0.55**	-0.85**	0.2	0.77**	-0.98**	0.28	-0.74**	0.48**	0.78**	-0.96**	0.55**	-0.85**	0.2	0.77**	-0.98**	0.28
Ablation-season snow	-0.35*	0.87**	1**	-0.59**	0.82**	-0.54**	0.61**	1**	-0.66**	0.56**	-0.35*	0.87**	1**	-0.59**	0.82**	-0.54**	0.61**	1**	-0.66**	0.56**
Ablation-season meltwater	0.83**	-0.25	-0.49**	1**	-0.34*	0.88**	-0.07	-0.66**	1**	-0.17	0.83**	-0.25	-0.49**	1**	-0.34*	0.88**	-0.07	-0.66**	1**	-0.17
Ablation-season S_{in}	-0.28	-0.49**	-0.32*	-0.15	-0.41**	-0.22	-0.43**	-0.23	-0.17	-0.28	-0.28	-0.49**	-0.32*	-0.15	-0.41**	-0.22	-0.43**	-0.23	-0.17	-0.28
Ablation-season albedo	-0.59**	0.53**	0.8**	-0.82**	0.62**	-0.78**	0.18	0.74**	-0.96**	0.28	-0.59**	0.53**	0.8**	-0.82**	0.62**	-0.78**	0.18	0.74**	-0.96**	0.28
Ablation-season S_{out}	0.66**	-0.2	-0.5**	0.79**	-0.32*	0.77**	0.3*	-0.53**	0.91**	-0.15	0.66**	-0.2	-0.5**	0.79**	-0.32*	0.77**	0.3*	-0.53**	0.91**	-0.15
Ablation-season L_{in}	0.82**	0.3*	0	0.66**	0.22	0.89**	0	0	0.78**	0.17	0.82**	0.3*	0	0.66**	0.22	0.89**	0	0.78**	0.78**	0.17
Ablation-season L_{out}	-0.88**	0.19	0.46**	-0.83**	0.26	-0.81**	0	0.53**	-0.77**	0	-0.88**	0.19	0.46**	-0.83**	0.26	-0.81**	0	0.53**	-0.77**	0
Ablation-season H_{sen}	0.32*	0	0	0.09	0.04	0.39**	0.35*	-0.3	0.41**	0	0.32*	0	0	0.09	0.04	0.39**	0.35*	-0.3	0.41**	0
Ablation-season H_{lat}	-0.02	0.56**	0.5**	-0.04	0.52**	-0.72**	0.25	0	0.38**	0.23	-0.02	0.56**	0.5**	-0.04	0.52**	-0.72**	0.25	0	0.38**	0.23

Meltwater is the positive value

* $p < 0.05$, and ** $p < 0.01$

sublimation/evaporation for the two glaciers (Table 1). After detrending, ablation-season snowfall explains 56% ($p < 0.05$) and 55% ($p < 0.05$) of the variance in annual mass balance, and ablation-season melt can explain 89% ($p < 0.05$) and 97% ($p < 0.05$) of the variance in annual mass balance for Qiyi and Ningchan No.1 glaciers (Fig. 6 and Table 2). Both the linear trend and interannual variability of data can contribute to the correlation between the two time-series data. When the linear trend is removed from the time series, the correlation coefficient can indicate the relationship between these data at interannual timescales. Thus, we selected to calculate the correlations between the detrended time series in this work to understand how climates impact interannual changes in mass balance. Above all, ablation-season melt is the most important component controlling the interannual changes in mass balance for both glaciers (Table 2).

3.4 The mass balance changes from 1970 to 2015

Interannual variability in mass balance is significant at the two glaciers (Fig. 3), with a maximum of 394 (or 605) mm w.e. in 1982/83 (or 1982/83) and a minimum of -842 (or -1543) mm w.e. in 2005/06 (or 2012/13) for Qiyi (or Ningchan No.1) Glacier. For the two glaciers, most of ablation-season mass balances are negative except for several years before 1993/94, and interannual fluctuation of ablation-season mass balance is highly consistent with that of annual mass balance during 1970–2015 (Fig. 6). Cold-season mass balances show small interannual variations, with values from -107 to 120 mm w.e. and from 162 to 345 mm w.e. on Qiyi and Ningchan No.1 glaciers, respectively (Fig. 6).

Despite some internal differences, interannual variations in mass balance are broadly synchronous at the two glaciers. After detrending, the two annual mass balance time series exhibit similar variations, with a correlation coefficient (r) of 0.61 ($p < 0.01$, Table 3). Such correlation mainly occurs in the ablation season (Fig. 6, $r = 0.65$, $p < 0.01$). We also evaluated the relationships of the annual mass balance of

glaciers in different parts of the Qilian Mountains. After detrending, correlation coefficients between the annual mass balance of the majority of selected glaciers in the Qilian Mountains are larger than 0.6 ($p < 0.01$, Table 3). The annual mass balances of glaciers from different regions of the Qilian Mountains show marked similarities at the interannual timescale.

Our study glaciers clearly show an overall decreasing mass balance trend ($p < 0.01$ via linear regression) during 1970–2015 (Fig. 3). According to the nonparametric Mann–Kendall test, the most likely abrupt change point occurred between 1993/94 and 1994/95 on Qiyi Glacier and between 1995/96 and 1996/97 on Ningchan No.1 Glacier. To compare the interdecadal variability, we divide our time series into two periods: 1970–1994 and 1995–2015 (Fig. 3). Student's t -tests, at 95% confidence level, reveal that the 1995–2015 period statistically differs from 1970 to 1994 on Qiyi ($p < 0.01$) and Ningchan No.1 ($p < 0.01$) glaciers. During 1970–1994, both glaciers had small negative or positive mass balances, and over 1995–2015 they both show strong mass loss (Fig. 3). Of the total mass loss during 1970–2015, the majority occurred during 1995–2015. The average annual mass balance during 1995–2015 was ~ 385 and ~ 778 mm w.e. a^{-1} smaller than that during 1970–1994 on Qiyi and Ningchan No.1 glaciers, respectively.

4 Discussion

4.1 Interannual glacier mass balance variability over the Qilian Mountains, and their relationships with climate and large-scale circulation

4.1.1 Climate factors controlling the interannual glacier mass balance changes across the Qilian Mountains

To quantify the effects of climate factors on interannual changes in glacier mass balances in the Qilian Mountains,

Table 3 The correlation coefficients (r) among mass balances for different glaciers using their detrending time series

Glacier 1	Glacier 2	Period	r
Qiyi (this study)	Ningchan No.1 (this study)	1970–2015	0.61 ($p < 0.01$)
Qiyi (this study)	Beida River catchment in the western Qilian Mountains (Wang et al. 2017)	1970–2013	0.84 ($p < 0.01$)
Qiyi (this study)	Laohugou No.12 Glacier in the western Qilian Mountains (Chen et al. 2020)	1970–2015	0.53 ($p < 0.01$)
Qiyi (this study)	Lenglongling region in the eastern Qilian Mountains (Cao et al. 2019)	1972–2015	0.66 ($p < 0.01$)
Qiyi (this study)	Shiyi Glacier in the middle Qilian Mountain (Zhang et al. 2021)	1970–2015	0.7 ($p < 0.01$)
Ningchan No.1 (this study)	Laohugou No. Glacier in the western Qilian Mountains (Chen et al. 2020)	1970–2015	0.6 ($p < 0.01$)
Ningchan No.1 (this study)	Lenglongling region in the eastern Qilian Mountains (Cao et al. 2019)	1972–2015	0.85 ($p < 0.01$)
Ningchan No.1 (this study)	Beida River catchment in the western Qilian Mountains (Wang et al. 2017)	1972–2013	0.68 ($p < 0.01$)
Ningchan No.1 (this study)	Shiyi Glacier in the middle Qilian Mountain (Zhang et al. 2021)	1970–2015	0.66 ($p < 0.01$)

we examine the relationships among ablation-season T_a , annual precipitation, and annual mass balance. After detrending the data, the annual mass balance of Qiyi and Ningchan No.1 glaciers demonstrate a weak correlation with annual precipitation at Tuole ($r=0.58$, $p<0.01$) and Menyuan ($r=0.3$, $p<0.05$) station, respectively. It is because annual precipitation plays a minor role in influencing interannual changes in the melt for the two glaciers (Table 2). Instead, the annual mass balance of Qiyi and Ningchan No.1 glaciers show a strong negative correlation with T_a in the ablation season from Tuole ($r=-0.71$, $p<0.01$) and Menyuan ($r=-0.8$, $p<0.01$) stations, respectively. We analyzed how ablation-season T_a impacts the interannual changes in mass balance for the two glaciers. For the two glaciers, the correlations between ablation-season T_a and snowfall are significant (Table 2), while the correlations between ablation-season T_a and precipitation are not significant (after detrending, $r=0.05$, $p>0.05$ for Qiyi Glacier; $r=0.05$, $p>0.05$ for Ningchan No.1 Glacier). These indicate that changes in ablation-season T_a can impact snowfall amount by changing the precipitation phase (or the ratio of snowfall to precipitation) because correlation (after detrending, $r=-0.6$, $p<0.05$ for Qiyi Glacier; $r=-0.72$, $p<0.05$ for Ningchan No.1 Glacier) between ablation-season T_a at Tuole (or Menyuan) station and the ratio of ablation-season glacier-wide snowfall to ablation-season glacier-wide precipitation for Qiyi (or Ningchan No.1) Glacier is significant (Fig. S3). In addition, ablation-season T_a can impact the changes in L_{in} for the two glaciers according to a significant positive correlation between these two variables (Fig. S3 and Table 2) which has also been found in some other studies (Ohmura 2001; Yang et al. 2001; Zhu et al. 2017). A good relationship between melt energy and L_{in} (Table 2) indicates L_{in} can affect changes in melt energy during the ablation season. Ablation-season melt energy linked to L_{in} can impact the changes in albedo and S_{out} by changing snow characteristics (such as snow thickness). Thus, ablation-season T_a also shows good relationships with ablation-season albedo and S_{out} (Table 2). For Ningchan No.1 Glacier, T_a can also affect melt energy by linking turbulent heat fluxes during the ablation season due to well relationships between T_a and turbulent heat fluxes, and between meltwater and turbulent heat fluxes (Table 2). However, the low correlations between turbulent heat fluxes and meltwater (Table 2) and small strengths (standard deviations) of interannual variability of turbulent heat fluxes indicate that the influence of changes in turbulent heat fluxes on melt energy during the ablation season is small for Ningchan No.1 Glacier. Above all, T_a mainly affects the snowfall (or precipitation phase) and L_{in} during the ablation season, which further influences albedo and melt for the two glaciers. In this way, ablation-season T_a controls the interannual changes in mass balance for the two glaciers.

We further analyze the relationships between the annual mass balance of Qiyi and Ningchan No.1 glaciers and regional climate variables from CN05.1. The mass balance of Qiyi and Ningchan No.1 glaciers is significantly negatively correlated with the ablation-season T_a in the northeast TP (Fig. S4). The annual mass balance of Qiyi Glacier during 1970–2015 showed a slight positive correlation with annual precipitation in most regions of the western Qilian Mountains (Fig. S4). However, the annual mass balance of Ningchan No.1 Glacier during 1970–2015 yields no obvious correlation with the annual precipitation across the Qilian Mountains (Fig. S4). In addition, the annual mass balance of Laohugou No.12 and Shiyi glaciers correlated with the ablation-season T_a in the northeast TP and showed no significant relationship with annual precipitation in the northeast TP (Fig. S5). These relationships also occurred for regionally-averaged glacier annual mass balances for the Beida River catchment in the western Qilian Mountains and Lenglongling Mountains in the eastern Qilian Mountains (Figure is now shown). Thus, interannual changes in mass balance of glaciers appear to be controlled mainly through ablation-season T_a variations in the Qilian Mountains.

4.1.2 Relationships between atmospheric circulation patterns and glacier mass balance across the Qilian Mountains

The correlation analysis is helpful in revealing the influence of atmospheric circulation on changes in climates and glacier mass balance (Mölg et al. 2014; Vuille et al. 2008; Zhu et al. 2021b). To explore the influence of large-scale dynamic processes on interannual changes in glacier mass balance across the Qilian Mountains, we correlate the regionally-averaged T_a index with geopotential height and wind fields at the 500 hPa level. The regionally-averaged T_a index is derived from the normalized ablation-season T_a averaged over the 10 stations along the Qilian Mountains (Fig. 1 and Table S3). The correlation coefficient between the regionally-averaged T_a index and the measured ablation-season T_a from all 10 stations is greater than 0.9 for each station. In addition, a strong positive correlation between the regionally-averaged T_a index and CN05.1 gridded ablation-season T_a data was found in the northeast TP (Fig. S6). After detrending, the correlation coefficients between the regionally-averaged T_a index and the reconstructed mass balance of Qiyi, Ningchan No.1, Laohugou No.12, and Shiyi glaciers and of regional glaciers in the Beida River catchment and Lenglongling Mountains are -0.69 , -0.8 , -0.75 , -0.71 , -0.76 , and -0.87 with $p<0.01$, respectively (Table 4). Thus, this regionally-averaged T_a index is highly representative of the consistent ablation-season T_a changes and glacier mass balance variations in the western and eastern Qilian Mountains.

Table 4 The correlation coefficients of ablation-season circulation indexes and annual mass balance of four glaciers during 1970–2015

Circulation indexes	Ningchan No.1	Lenglongling	Annual mass balance				Regionally-averaged T_a index
			Qiyi	Beida River	Shiyi	Laohugou No.12	
Regionally-averaged T_a index							
Without detrending	− 0.89** (− 0.95**)	− 0.91** (− 0.95**)	− 0.77** (− 0.88**)	− 0.84** (− 0.93**)	− 0.69** (− 0.7**)	− 0.88** (− 0.94**)	1** (1**)
After detrending	− 0.8** (− 0.87**)	− 0.87** (− 0.88**)	− 0.69** (− 0.81**)	− 0.76* (− 0.83**)	− 0.71** (− 0.71**)	− 0.75** (− 0.77**)	1** (1**)
Regionally-averaged geopotential height over northern central China (30° N–45° N, 90° E–130° E)							
Without detrending	− 0.68** (− 0.82**)	− 0.71** (− 0.82**)	− 0.61** (− 0.79**)	− 0.69** (− 0.83**)	− 0.54** (− 0.59**)	− 0.72** (− 0.9**)	0.81** (− 0.9**)
After detrending	− 0.47** (− 0.52**)	− 0.56** (− 0.53**)	− 0.47** (− 0.55**)	− 0.52* (− 0.54**)	− 0.45** (− 0.41**)	− 0.52** (− 0.68**)	0.68** (− 0.69**)
Regionally-averaged geopotential height over Europe (55° N–65° N, 15° E–50° E)							
Without detrending	− 0.65** (− 0.79**)	− 0.69** (− 0.84**)	− 0.51** (− 0.78**)	− 0.56** (− 0.79**)	− 0.52** (− 0.65**)	− 0.51** (− 0.69**)	0.64** (− 0.8**)
After detrending	− 0.57** (− 0.67**)	− 0.61** (− 0.67**)	− 0.39** (− 0.64**)	− 0.46** (− 0.61**)	− 0.45** (− 0.54**)	− 0.36** (− 0.48**)	0.57** (− 0.73**)
K–KE index							
Without detrending	− 0.68** (− 0.86**)	− 0.66** (− 0.87**)	− 0.56** (− 0.76**)	− 0.63** (− 0.67**)	− 0.41** (− 0.58**)	− 0.67** (− 0.82**)	0.74** (− 0.88**)
After detrending	− 0.54** (− 0.72**)	− 0.52** (− 0.71**)	− 0.42** (− 0.56**)	− 0.48** (− 0.52**)	− 0.3* (− 0.41**)	− 0.52** (− 0.64**)	0.64** (− 0.79**)

The values in the brackets are the correlation coefficients after a three-year running mean was used for ablation-season mass balances on four glaciers and circulation indexes

** $p < 0.01$; * $p < 0.05$

Spatial patterns of correlations between the regionally-averaged T_a index and JRA55 gridded geopotential height/wind fields at 500 hPa in the ablation season during 1970–2015 reveal distinct centers of strong correlation from Europe to the Northwest Pacific (Fig. 7). A higher T_a in the Qilian Mountains corresponds to higher 500 hPa geopotential heights and anomalous anticyclonic circulation in northern central China, Europe and the Northwest Pacific, and to lower 500 hPa geopotential heights and anomalous cyclonic circulation in central Asia (Fig. 7). Two distinct processes may jointly influence interannual changes in ablation-season T_a in the Qilian Mountains. Some studies have found that the combined effects (Li et al. 2019b) or interactions (Mölg

et al. 2017; Yao et al. 2019) of different circulations play an important role in regional climate changes. The first process could be linked to the Europe-Asia teleconnection. The correlation fields between the 500 hPa regionally-averaged geopotential height over Europe (55°–65° N, 15° E–50° E) and JRA55 gridded geopotential height/wind fields at 500 hPa in the ablation season during 1970–2015 (Fig. 8a) show similar wave trains from Europe to northern central China (Fig. 7), illustrating that atmospheric circulation anomalies in Europe can impact those in the Qilian Mountains. Such wave-train enables the transfer of perturbation energy from the North Atlantic/Europe to eastern Asia, associated with the jet stream (Bothe et al. 2011; Li and Ruan 2018; Ding

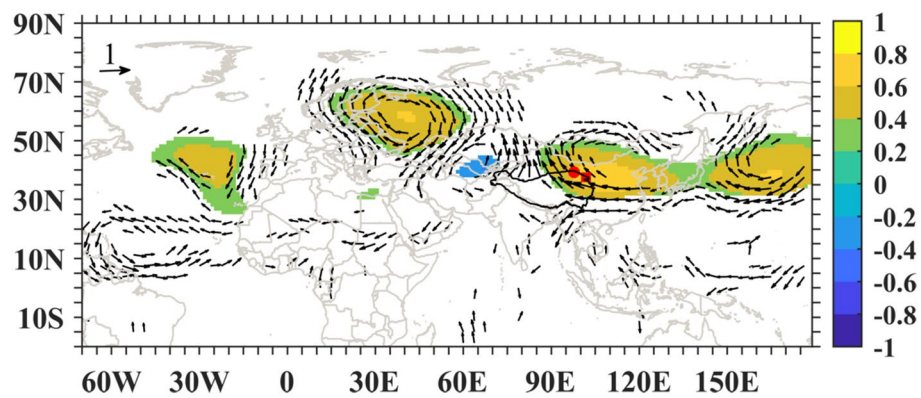
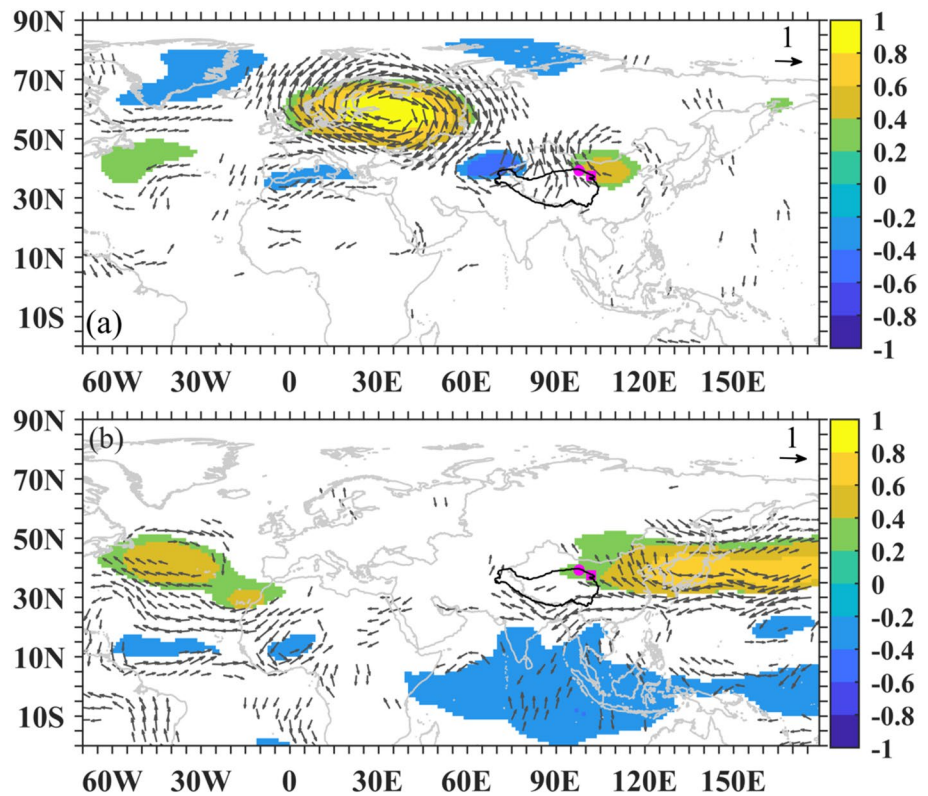


Fig. 7 Correlation fields between detrended JRA55 gridded geopotential height (gpm) fields/wind fields at 500 hPa and detrended regionally-averaged air temperature index during the ablation season from 1970 to 2015. The correlations of the 500 hPa geopotential

height fields and wind fields (either zonal or meridional wind speed) are plotted only when correlations are significant at the 0.05 level. The red dot and red square denote Qiyi and Ningchan No.1 glaciers, respectively

Fig. 8 Correlation patterns of detrended JRA55 gridded geopotential height (gpm)/wind fields at 500 hPa height with the detrended 500 hPa regionally-averaged geopotential height over Europe (55°–65° N, 15° E–50° E) (a) and the detrended regionally-averaged sea surface temperature over Kuroshio and its extension area (25° N–45° N, 120° E–180° E) in the Northwest Pacific (b) during the ablation season from 1970 to 2015 using the Pearson correlation analysis. The correlations of the 500 hPa geopotential height and wind fields (either zonal or meridional wind speed) are plotted only when correlations are significant at the 0.05 level. The pink dot and pink square denote Qiyi and Ningchan No.1 glaciers, respectively



and Wang 2005; Mölg et al. 2014; Saeed et al. 2011). Similarly, Mölg et al. (2017) found that atmospheric circulation patterns comprising an anticyclonic anomaly over Europe and a cyclonic anomaly over central Asia can cause high T_a in the east TP (including the Qilian Mountains). This previous study considered that with increasing distance from the center of a cyclonic anomaly over central Asia, stronger advection of warm air where southerlies meet the expansion zone of the South Asian High would promote warming

across the east TP (Mölg et al. 2017). Likewise, interannual changes in ablation-season T_a across the Qilian Mountains appear to have a close linkage with atmospheric circulation anomalies in Europe, through mid-latitude wave trains over Eurasia. Zhang et al. (2021) also found that climate changes in Europe exert influences on T_a on Shiyi Glacier in the central Qilian Mountains. In addition, after detrending, the ablation-season regionally-averaged geopotential height over northern central China (30° N–45° N, 90° E–130° E)

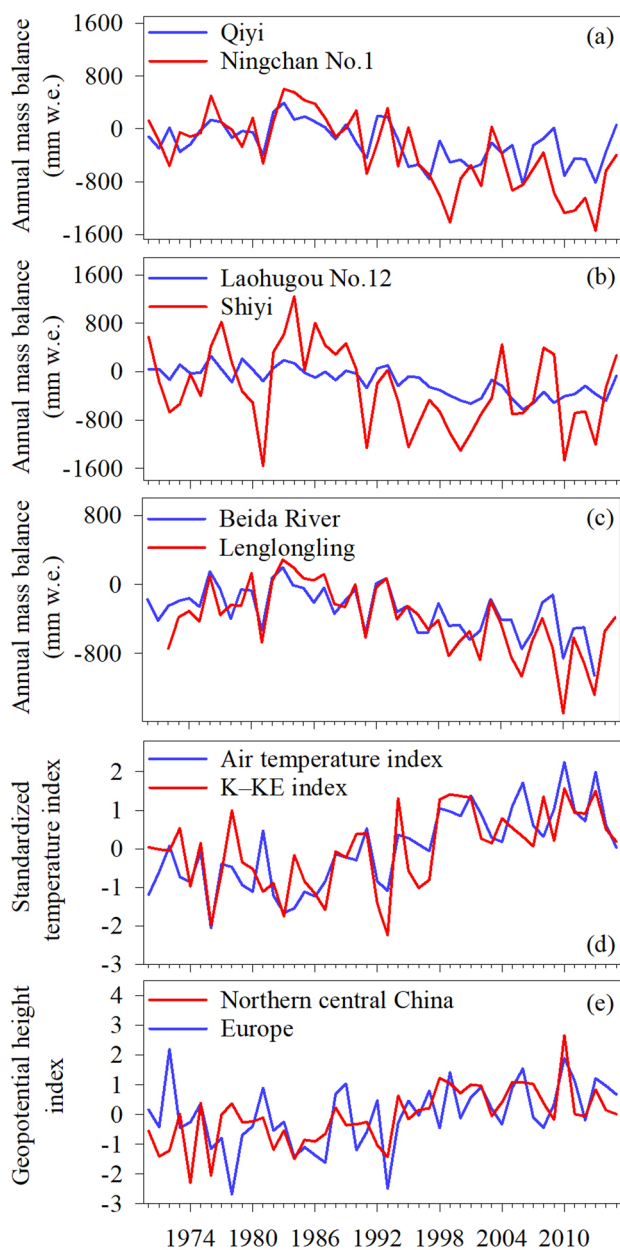


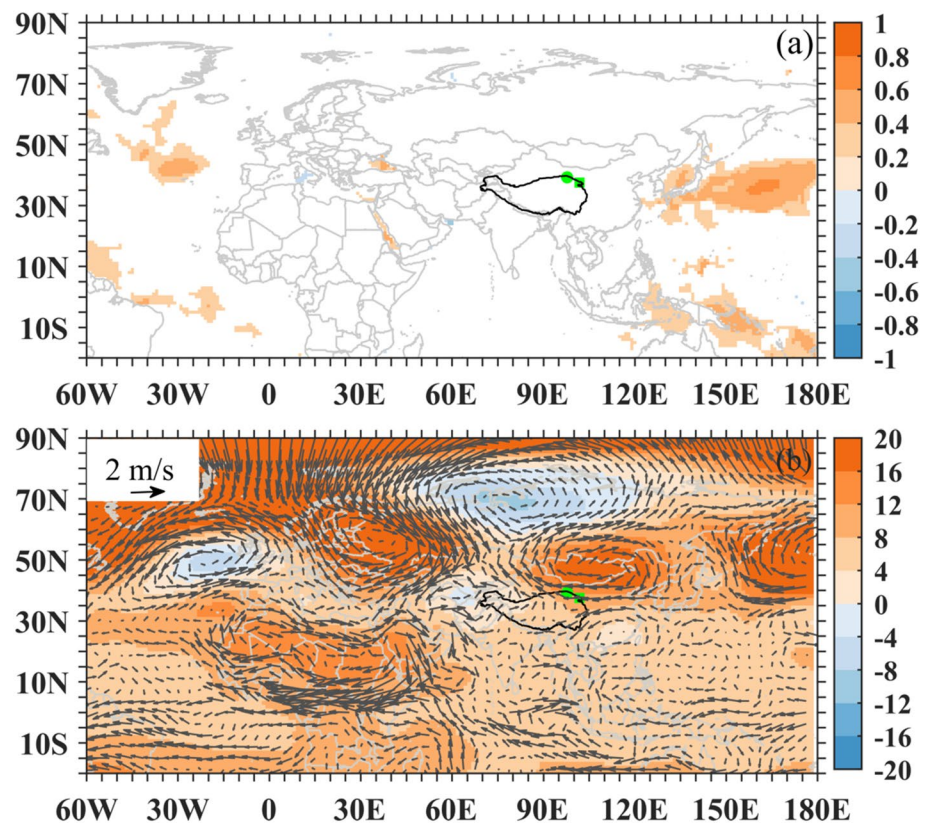
Fig. 9 Annual mass balance of **a** Qiyi and Ningchan No.1, **b** Laohugou No.12 (Chen et al. 2020) and Shiyi (Zhang et al. 2021) glaciers, and **c** regional glaciers in the Beida River catchment (Wang et al. 2017) and Lenglongling Mountains (Cao et al. 2019); **d** ablation-season regionally-averaged air temperature over the Qilian Mountains and sea surface temperature over the Kuroshio and its extension area (25° N– 45° N, 120° E– 180° E) in the Northwest Pacific; and **e** standardized ablation-season 500 hPa regionally-averaged geopotential height over northern central China (30° – 45° N, 90° E– 130° E) and over Europe (55° N– 65° N, 15° E– 50° E) from 1970 to 2015

(or over Europe (55° N– 65° N, 15° E– 50° E)) is significantly correlated with the regionally-averaged T_a index, and the modelled annual mass balance of Qiyi, Ningchan No.1, Laohugou No.12, Shiyi glaciers and of regional glaciers in

the Beida River catchment and Lenglongling Mountains (Table 4 and Fig. 9). Thus, interannual changes in mass balance and ablation-season T_a across the Qilian Mountains appear to have a close linkage with atmospheric circulation anomalies in the European region through a wave train of cyclonic and anticyclonic anomalies over Eurasia.

The second factor involves atmospheric circulation changes over the Northwest Pacific, which are connected to the anticyclonic anomaly in northern central China through Northwest Pacific-Asia teleconnection (Fig. 7). Ding et al. (2019) suggested that the anomalous high SSTs over Kuroshio and its extension area (K-KE) in the Northwest Pacific are favorable for the formation of anomalous positive geopotential heights and anticyclones in the Northwest Pacific, by enhancing convection over the Northwest Pacific. The K-KE index is defined as the SST averaged over 25° N– 45° N, 120° E– 180° E, which indicates the changes in SST over the K-KE (Ding et al. 2019). The correlations between the K-KE index and the JRA55 gridded geopotential height/wind fields at 500 hPa in the ablation season during 1970–2015 indicate that anomalous high SSTs over the K-KE area are favorable for the formation of anomalous positive geopotential height and anticyclonic circulation in the Northwest Pacific and northern central China (Fig. 8b). This finding illustrates that the changes in SSTs over the K-KE area can impact atmospheric circulation and thus T_a in the Qilian Mountains. A positive relationship between regionally-averaged T_a index and SSTs over the K-KE area (Fig. 10a) verifies that high SSTs over the K-KE area are favorable for the high T_a over the Qilian Mountains. Furthermore, the ablation-season K-KE index is significantly correlated with the regionally-averaged T_a index, and also with the modelled annual mass balance of Qiyi, Ningchan No.1, Laohugou No.12, and Shiyi glaciers and of regional glaciers in the Beida River catchment and Lenglongling Mountains during 1970–2015 (Table 4 and Fig. 9c). In addition, the measured mass balance of Qiyi, Ningchan No.1, Laohugou No.12, and Shiyi glaciers also show correlations with regionally-averaged T_a index, regionally-averaged geopotential height over northern central China, regionally-averaged geopotential height over Europe and K-KE index (Table S4). Please note that the short data series (5 or 6 years) prevent the correlations from being significant between regionally-averaged geopotential height over Europe and Ningchan No.1 (or Shiyi) Glacier, and the correlations are more significant for Qiyi Glacier which has a relative long-term measured annual mass balance. Overall, the combination of changes in atmospheric circulation in Europe and SST in Kuroshio and its extension area of the Northwest Pacific affect interannual changes in glacier mass balance across the Qilian Mountains by critically influencing interannual variation of T_a during the ablation season.

Fig. 10 **a** Correlation fields ($p < 0.05$) between detrended sea surface temperature and detrended regionally-averaged air temperature index during the ablation season from 1970 to 2015 using the Pearson correlation analysis. **b** Differences in the mean 500 hPa geopotential heights (gpm) and wind speed field from JAR55 between 1995–2015 and 1970–1994 during the ablation season (June–September) (1995–2015 minus 1970–1994). The green dot and green square denote Qiyi and Ningchan No.1 glaciers, respectively



4.2 Regional climate variables driving interdecadal changes of glacier mass balance across the Qilian Mountains

4.2.1 Representativeness of the topographic characteristics of the studied glaciers

For glaciers in the Qilian Mountains, glaciers with areas $< 1.0 \text{ km}^2$ accounted for the largest number of glaciers, while glaciers with areas in the range of $1.0\text{--}5.0 \text{ km}^2$ accounted for the most glacierized area in the Qilian Mountains (Sun et al. 2018a). And the average glacier area in the entire Qilian Mountain is 0.6 km^2 (Sun et al. 2018a). The average glacier area is 0.33 and 0.46 km^2 for the selected 161 glaciers in the eastern Qilian Mountains and is 0.46 km^2 for the selected 688 glaciers in the western Qilian Mountains (Fig. S7). The area of Qiyi (or Ningchan No.1) Glacier is not smaller when compared to other glaciers in the Qilian Mountains. In addition, there are 74 glaciers with areas $> 1.0 \text{ km}^2$ and 27 glaciers with areas $> 2.0 \text{ km}^2$ in the western Qilian Mountains, while there are 16 glaciers with areas $> 1.0 \text{ km}^2$ and 3 glaciers with areas $> 2.0 \text{ km}^2$ in the eastern Qilian Mountains. The area of the largest glacier is smaller than 3 km^2 in the eastern Qilian Mountains and is more than 20 km^2 in the western Qilian Mountains. Above all, the western Qilian Mountains have more large glaciers and a higher

average glacier area when compared to the eastern Qilian Mountains. The area of Qiyi Glacier is also larger than that of Ningchan No.1 Glacier.

Hypsography is another topographic variable that may impact multidecadal averages and variability of individual and regional glacier mass balance (Brun et al. 2019; Zhu et al. 2018b). Glaciers in the eastern Qilian Mountains are distributed at relatively lower altitudes than glaciers in the western Qilian Mountains (Fig. S8), due to higher precipitation in the eastern Qilian Mountains (Table S3). The median elevation of glaciers (where elevation divides glacier area equally) is presumed to be at the equilibrium-line altitude, such that mass balance is zero at that elevation (Sakai et al. 2015). The median elevation provides a good index to understand the difference in altitude distribution of glaciers in different regions of the TP. The median elevations were 4780 and 4400 m a.s.l. for Qiyi and Ningchan No.1 glaciers, respectively. The median elevations were 4820 m a.s.l. for 682 selected glaciers in the western Qilian Mountains and 4500 m a.s.l. for 169 selected glaciers in the eastern Qilian Mountains (Figs. S7 and S8). Thus, the difference of median elevations between Qiyi and Ningchan No.1 glaciers was 380 m a.s.l., which is similar to the difference between the larger sets of glaciers in the western and eastern Qilian Mountains (320 m a.s.l.).

Table 5 The seasonal meteorological variable at stations and seasonal glacier-wide mass balance components in different periods for Qiyi and Ningchan No.1 glaciers

Scale	Variable	Qiyi						Ningchan No.1						
		1970–1994			1995–2015			1970–1994			1995–2015			
		Cold	Ablation	Annual	Cold	Ablation	Annual	Cold	Ablation	Annual	Cold	Ablation	Annual	
Stations	Precipitation (mm)	58	242	300	60	263	323	263	9.2	323	378	537	366	517
	T_a (°C)	-8.3	7.9	-2.9	-7.3	9.2	-1.8	9.2	-4.1	10.1	10.1	0.6	11.2	1.7
	RH (%)	42	58	48	40	56	45	56	43	58	48	48	56	45
	T_a (°C)	-18.4	-2.2	-13.0	-17.4	-0.9	-11.9	-0.9	-13.7	0.5	0.5	-9.0	1.5	-8.0
Glacier-wide (mm w.e. a ⁻¹)	Mass balance	8	-40	-32	-13	-412	-425	-412	252	-237	15	15	-992	-763
	Snowfall	87	317	404	91	300	391	300	267	391	658	658	303	557
	Refreezing	3	121	124	5	129	134	129	33	187	220	220	146	181
	Sublimation	-62	-59	-121	-78	-69	-147	-69	-30	-18	-48	-48	-13	-42
	Melt	-20	-419	-439	-31	-772	-803	-772	-18	-797	-815	-815	-1428	-1459
	Rain	0	47	47	0	95	95	95	3	251	254	254	318	323
	Precipitation	87	364	451	91	395	486	395	270	642	912	912	621	879
	Ratio of snowfall to precipitation	1	0.87	0.9	1	0.76	0.8	0.76	0.99	0.61	0.72	0.72	0.49	0.63

4.2.2 Regional climate variables driving the increase in glacier mass loss rate across the Qilian Mountains during 1970–2015

The mean annual mass balance during 1995–2015 was more negative on Qiyi and Ningchan No.1 glaciers than during 1970–1994 due to higher ablation-season meltwater during 1995–2015 (Fig. 3 and Table 5). Differences in ablation-season S_{in} , H_{sen} , H_{lat} and G between 1970–1994 and 1995–2015 were small for the two glaciers (Table 6). The absolute values of L_{out} and QPS during 1995–2015 were higher than those during 1970–1994, indicating that changes in these two components can not contribute to the higher absolute value of melt energy during 1995–2015 (Table 6). Thus, differences in L_{in} and S_{out} related to albedo caused different melt energy in the ablation season between 1970–1994 and 1995–2015 for the two glaciers. According to the most parameterizations for L_{in} (Crawford and Duchon 1999; Yang et al. 2001; Zhu et al. 2017), we can find that L_{in} can be influenced by cloud cover, T_a , and humidity. The cloud cover is always calculated using the ratio of the S_{in} to the incoming shortwave radiation at the top of the atmosphere (S_{TOA}), such as $n = 1 - (S_{in}/S_{TOA})$ (Crawford and Duchon 1999) and $n = 1.3 - 1.4(S_{in}/S_{TOA})$ (Favier et al. 2004b). For the two glaciers, the difference in ablation-season S_{in} between 1970–1994 and 1995–2015 was small (Table 6), indicating that cloud cover was similar between the two periods. And the difference in ablation-season RH between 1970–1994 and 1995–2015 was also small (Table 5). From 1970–1994 to 1995–2015, ablation-season glacier-wide precipitation was increased for Qiyi Glacier and was slightly reduced for Ningchan No.1 Glacier, however, ablation-season glacier-wide snowfall was slightly decreased for Qiyi Glacier and was significantly decreased for Ningchan No.1 Glacier due to less precipitation falling as snow (Fig. 6 and Table 5). Thus, higher T_a led to higher L_{in} , and less snowfall in the ablation season for the two glaciers during 1995–2015 when compared to 1970–1994 (Tables 5 and 6). From 1970–1994 to 1995–2015, the decreased snowfall and increased melt related to increased L_{in} can cause the decreased albedo in the ablation season, which furtherly increased melt for the two glaciers. Thus, through increasing L_{in} and reducing snowfall, the increased ablation-season T_a was considered as the primary cause of lower mass balance during 1995–2015 when compared to 1970–1994.

We furtherly evaluate the contributions of changing ablation-season T_a and annual precipitation to changes in mass balance from 1970–1994 and 1995–2015 for Qiyi and Ningchan No.1 glaciers using sensitivity analysis (Table S5). To account for the difference in mean ablation-season T_a between 1970–1994 and 1995–2015 at Qiyi and Ningchan No.1 glaciers, the EMB model was rerun with -1.3 and -1.1 °C changes in the daily mean T_a in the

Table 6 The glacier-wide energy balance components ($W m^{-2}$) in the ablation season for different periods on Qiyi and Ningchan No.1 glaciers

	Qiyi			Ningchan No.1		
	1970–1994	1995–2015	1970–2015	1970–1994	1995–2015	1970–2015
S_{in}	220	220	220 (8)	241	235	238 (7)
a	0.66	0.59	0.63	0.7	0.59	0.65
S_{out}	– 146	– 130	– 139 (10)	– 169	– 138	– 155 (14)
S_{net}	74	90	81 (9)	72	97	83 (12)
L_{in}	255	262	258 (4)	261	268	264 (4)
L_{out}	– 300	– 306	– 303 (2)	– 307	– 310	– 308 (2)
L_{net}	– 45	– 44	– 45 (3)	– 46	– 42	– 44 (3)
H_{sen}	5	6	6 (1)	6	5	6 (1)
H_{lat}	– 15	– 18	– 16 (3)	– 4	– 3	– 4 (1)
QPS	– 9	– 13	– 11 (2)	– 9	– 14	– 11 (3)
G	3	3	3 (2)	6	2	4 (2)
Q_M	13	24	18 (7)	25	45	34 (10)
T_S	– 3.5	– 2.2	– 2.9	– 1.9	– 1.2	– 1.6

The values in the bracket are standard deviations of the detrending variables
 T_S is glacier surface temperature

ablation season during 1995–2015 for Qiyi and Ningchan No.1 glaciers, respectively. T_a in other periods, and other variables, remained unchanged. The recalculated average annual mass balance during 1995–2015 is similar to the average annual mass balance during 1970–1994 for Qiyi and Ningchan No.1 glaciers (Table S5), indicating that increasing ablation-season T_a accounted for almost all the mass loss from 1970–1994 and 1995–2015. In addition, the EMB model was rerun with a – 7.1% and 3.9% change in daily precipitation during 1995–2015 on Qiyi and Ningchan No.1 glaciers, respectively, to calculate the contribution of annual precipitation change to mass balance change from 1970–1994 and 1995–2015 (Table S5). The corresponding deviations for mean annual mass balances during 1995–2015 resulting from the precipitation variability are only – 77 and 62 mm w.e. a^{-1} for Qiyi and Ningchan No.1 glaciers, respectively. The results confirm that higher ablation-season T_a was the main driver of the greater mass loss during 1995–2015 than during 1970–1994 at the two glaciers, and of the higher mass-loss rate of Ningchan No.1 Glacier compared to Qiyi Glacier.

The influence of increased ablation-season T_a on increasing glacier mass loss from 1970–1994 to 1995–2015 is mainly attributed to two processes: first the reduction in precipitation falling as snow, and second the enhanced melt from increasing L_{in} and associated feedbacks. We further estimated the contributions of these two processes to the increasing mass loss of the two glaciers (Table S6). Our data show that 43% (or 63%) and 33% (or 22%) of the increased mass loss from 1970–1994 to 1995–2015 result from reduced precipitation falling as snow and increasing L_{in} on Qiyi (or Ningchan No.1) Glacier, respectively (Table S6). Under the influence of increased T_a from 1970–1994 to

1995–2015, the reduction in precipitation falling as snow plays a more important role in the increased mass loss from 1970–1994 to 1995–2015 when compared to the enhanced melt from increasing L_{in} . In addition, under similar warming conditions, the influence of reduced precipitation falling as snow on mass balance change is more significant for Ningchan No.1 Glacier than for Qiyi Glacier.

All stations near the Qilian Mountains show that ablation-season T_a during 1995–2015 was about 1 °C higher than during 1970–1994 (Table S3). Yuan et al (2021) also indicated that the northern TP, including Qilian Mountains, had the highest warming rate during the last several decades. In addition, ablation-season L_{in} increased, ablation-season snowfall and the ratio of ablation-season snowfall to ablation precipitation decreased from 1970–1994 to 1995–2015 across the Qilian Mountains (Fig. S9). Meanwhile, the reduced ablation-season snowfall was larger in the eastern Qilian Mountains than in the western Qilian Mountains (Fig. S9). These variations can cause the accelerated glacier mass loss in the Qilian Mountains from the 1970s–1990s to 1990s–2010s. This view is verified by the reconstructed mass balances for single glaciers and regional glaciers in different regions of the Qilian Mountains (Fig. 9). The increased ablation-season T_a over the Qilian Mountains from 1970–1994 to 1995–2015 was caused by positive 500 hPa geopotential height anomalies in Europe (Fig. 10b; Zhang et al. 2021) and higher ablation-season SST in Kuroshio and its extension area of the Northwest Pacific during 1995–2015 (Fig. 9c) through teleconnections, as stated above. Besides the above atmospheric circulation, anthropogenic forcing, including anthropogenic greenhouse gases and aerosol emissions, are also important in inducing the warming on the TP over the last several decades (Yao et al. 2019).

4.2.3 Differences in interdecadal mass changes between Qiyi and Ningchan No.1 glaciers

The mass balance change rate (MBCR) is defined as that mean annual mass balance during 1995–2015 minus that during 1970–1994. The MBCR is -778 mm w.e. a^{-1} at Ningchan No.1 Glacier, which is 385 mm w.e. a^{-1} lower than that at Qiyi Glacier (Table 5). As stated above, from 1970–1994 and 1995–2015, a 1 °C increase in ablation-season T_a at the two glaciers has led to higher mass-loss rates at Ningchan No.1 Glacier than at Qiyi Glacier. This means that the mass balance sensitivity to T_a change is higher at Ningchan No.1 Glacier than at Qiyi Glacier. Oerlemans et al (1998) and Liu and Liu (2016) found that the higher sensitivity to T_a change may result from a lower glacier area-altitude distribution. And glacier area-altitude distribution at Ningchan No.1 Glacier is lower than at Qiyi Glacier. Thus, we thought that different glacier hypsography is a factor causing larger mass loss at Ningchan No.1 Glacier than at Qiyi Glacier between 1970–1994 and 1995–2015. To test this point, we reran the EMB model for Qiyi Glacier with the area-altitude of Ningchan No.1 Glacier, and for Ningchan No.1 Glacier with the area-altitude of Qiyi Glacier. To remove the influence of decreased ablation-season precipitation from 1970–1994 and 1995–2015 on mass balance change for Ningchan No.1 Glacier, daily precipitation in the ablation season during 1995–2015 at Menyuan station was multiplied by 1.122 to make mean ablation-season precipitation during 1995–2015 1.087 times larger than that during 1970–1994, reflecting differences at Tuole station between these periods. These recalculations show differences in mass balance between 1970–1994 and 1995–2015 of -548 mm w.e. a^{-1} for Qiyi Glacier and -218 mm w.e. a^{-1} for Ningchan No.1 Glacier (Table S5), and the new MBCR is 330 mm w.e. a^{-1} higher at Ningchan No.1 Glacier than at Qiyi Glacier. This finding is contrary to the result from the control run, in which MBCR is 385 mm w.e. a^{-1} lower at Ningchan No.1 Glacier than that at Qiyi Glacier. The results confirm that lower glacier area-altitude distribution is the largest contributor causing larger mass loss at Ningchan No.1 Glacier than Qiyi Glacier between 1970–1994 and 1995–2015, accounting for 330 mm w.e. a^{-1} of the 385 mm w.e. a^{-1} larger mass loss at Ningchan No.1 Glacier from 1970–1994 and 1995–2015 when compared to Qiyi Glacier. The explanation for this result is that a higher glacier area-altitude distribution for Qiyi Glacier can cause more precipitation to fall as snow, therefore leading to higher albedo and lower melt energy in the ablation season on Qiyi Glacier when compared to Ningchan No.1 Glacier (Table S7).

In addition, the mean ablation-season glacier-wide precipitation was 32 mm a^{-1} higher during 1995–2015 than 1970–1994 on Qiyi Glacier, while it was 21 mm a^{-1} lower

during 1995–2015 than 1970–1994 at Ningchan No.1 Glacier (Table 5). Such different ablation-season precipitation change can also play a role in the higher mass-loss rate of Ningchan No.1 Glacier than Qiyi Glacier from 1970–1994 and 1995–2015. To support the above interpretation, we carried out a sensitivity analysis for Ningchan No.1 Glacier. We reran the EMB model for Ningchan No.1 Glacier with daily precipitation in the ablation season at Menyuan station during 1995–2015 multiplied by 1.122, while keeping other variables unchanged. This adjustment makes the precipitation change from 1970–1994 and 1995–2015 similar at the two glaciers. The recalculated MBCR is 62 mm w.e. a^{-1} higher than that from the control run on Ningchan No.1 Glacier (Table S5). The results show that the difference in ablation-season precipitation changes from 1970–1994 and 1995–2015 contributes a small part (62 mm w.e. a^{-1}) of the difference in MBCR (385 mm w.e. a^{-1}) between Ningchan No.1 and Qiyi glaciers.

4.2.4 Spatial differences in interdecadal glacier mass changes between the western and eastern Qilian Mountains

Considering that ablation-season T_a is about 1 °C higher during 1995–2015 than during 1970–1994 at 10 stations across the Qilian Mountains (Table S3), we furtherly analyze the spatial difference in regional glacier hypsography (area–elevation distribution) and seasonal precipitation changes to obtain the knowledge about spatial differences in interdecadal changes in glacier mass balance between the western and eastern Qilian Mountains. According to the statement in Sect. 4.2.1, we find that glaciers in the eastern Qilian Mountains are distributed at relatively lower altitudes than glaciers in the western Qilian Mountains (Figs. S7 and S8). And the difference of median elevations between the larger sets of glaciers in the western and eastern Qilian Mountains is similar to that (380 m a.s.l.) between Qiyi and Ningchan No.1 glaciers.

In addition, the mean ablation-season precipitation during 1995–2015 was higher than that during 1970–1994 in the western Qilian Mountains, while mean precipitation in the ablation season (especially in June–August) for 1995–2015 was lower than that during 1970–1994 in the eastern Qilian Mountains (Table S3). Those spatial differences in interdecadal change of ablation-season precipitation in the western and eastern Qilian Mountains were caused by different regional atmospheric circulation changes between the two regions. Figure 10b reveals that the eastern boundary of the TP appears to have been dominated by stronger easterly wind anomalies during 1995–2015 compared with 1970–1994. This circulation pattern reduces water vapor on the TP which can export along the eastern boundary of the TP (Zhou et al. 2019). Thus, higher water vapor can remain

on the TP during 1995–2015 than 1970–1994. The warmer and wetter conditions on the TP made the atmosphere more unstable, triggering deeper convective cloud systems, which yielded more precipitation in the western Qilian Mountains during 1995–2015 compared with 1970–1994 (Yang et al. 2014). Figure 10b also shows that northerly air flow anomalies at the eastern margin of the southern TP indicate weaker southerly winds during 1995–2015 than during 1970–1994, which reduced the monsoonal moisture arriving into the eastern Qilian Mountains. These patterns may be related to a weakening of the Asian Summer Monsoon (Yang et al. 2014; Yao et al. 2012).

Therefore, we can deduce that the lower glacier area-altitude distribution and the reduction of ablation-season precipitation can favor the larger glacier mass loss rate from 1970–1994 and 1995–2015 in the eastern Qilian Mountains when compared to glaciers in the western Qilian Mountains. This view is verified by that the regionally-averaged glacier mass balance was about 520 mm w.e. a^{-1} lower during 1995–2013 than during 1972–1994 in the Lenglongling Mountains, in the eastern Qilian Mountains (Cao et al. 2019), while the average glacier mass balance was about 340 mm w.e. a^{-1} lower during 1995–2013 than during 1972–1994 in the Beida River catchment of the western Qilian Mountains (Wang et al. 2017) (Fig. 9c).

5 Conclusion

Time-series of mass balance from 1970 to 2015 on Qiyi Glacier in the western Qilian Mountains and on Ningchan No.1 Glacier in the eastern Qilian Mountains were reconstructed using the EMB model. The model was calibrated by in-situ mass balance data and validated by parts of measured mass balance data, modelled mass balance data from the published papers, and geodetic mass balance data. Based on our study and published glacier mass balance data, we find that interannual changes in glacier mass balance generally follow similar patterns across the Qilian Mountains, which are primarily related to changes in ablation-season T_a , because T_a mainly affects snowfall (precipitation phase) and L_{in} , which further influences albedo and melt. Such consistent interannual changes of glacier mass balance can be linked to the combination of changes in atmospheric circulation in Europe and SST in the Kuroshio and its extension area of the Northwest Pacific by changing ablation-season T_a . In addition, the average glacier mass balance was more negative during 1995–2015 than during 1970–1994 across the Qilian Mountains, because higher ablation-season T_a drove lower snowfall (with more precipitation falling as rain) and larger L_{in} , both of which contributed to lower surface albedo and higher melt energy during 1995–2015. The higher ablation-season T_a during 1995–2015 than during 1970–1994

appears to be linked with positive ablation-season 500 hPa geopotential height and anticyclonic anomalies in Europe and higher ablation-season SST in the Northwest Pacific in 1995–2015. Lastly, glacier mass loss rates were higher in the eastern Qilian Mountains than in the west from 1970–1994 and 1995–2015, mainly due to the lower glacier area-altitude distribution, as well as the reduction in ablation-season precipitation, in the eastern Qilian Mountains. This work hopes to provide a method or thinking to comparative analyze the spatiotemporal variability of glacier mass balance in different regions of the same glacierized massif on the TP and its surrounding areas associated drivers. We should note here that our results are mainly based on the modelled mass balance of only several typical glaciers across the Qilian Mountains. Long-term glacier mass balance monitoring is required to study the complex relationship between glaciers and climate in the Qilian Mountains and other regions (Wagnon et al. 2013; Yao et al. 2012). And the combination of multi-source data (reanalysis data, measured meteorological and glaciological data, and remote sensing data) with glacier models, the regional glacier mass balance in the Qilian Mountains or another glacierized massif can be reconstructed in future studies, which will help to improve the knowledge of the spatiotemporal patterns of glacier mass balance and meltwater on the TP.

Supplementary Information The online version contains supplementary material available at <https://doi.org/10.1007/s00382-022-06283-4>.

Funding This work was funded by Second Tibetan Plateau Scientific Expedition and Research Program (Grant no. 2019QZKK0201); Strategic Priority Research Program of Chinese Academy of Sciences (Grant no. XDA2006020102); National Natural Science Foundation of China (Grant no. 41971092, 41971092, 41771085 and 41801034); “Key Research Programs in Frontier Sciences” of the Chinese Academy of Sciences (Grant no. QYZDY-SSW-DQC003); National Science Foundation Paleo Perspectives on Climate Change (Grant no. 1502919); National Key Research and Development Project (2019YFC1509102).

Data availability We thank the National Tibetan Plateau/Third Pole Environment Data Center (<http://data.tpdc.ac.cn/>) and China Meteorological Administration (<http://data.cma.cn/>) for providing the climate data and some glacier-related data used herein. We are grateful to Xuejie Gao at the Institute of Atmospheric Physics, Chinese Academy of Sciences for providing CN05.1 data. JRA-55 reanalysis data sets are freely distributed on the National Center for Atmospheric Research (<http://rda.ucar.edu/datasets/ds628.1/>). The monthly sea surface temperature (SST) from the Hadley Centre Sea Ice and Sea Surface Temperature dataset (HadISST) can be downloaded from <https://www.metoffice.gov.uk/hadobs/hadisst/>. The SRTM DEM data and Landsat data are provided by the US Geological Survey (<https://earthexplorer.usgs.gov/>). This study is jointly funded by the Second Tibetan Plateau Scientific Expedition and Research Program (2019QZKK0201), the Strategic Priority Research Program of Chinese Academy of Sciences (Grant XDA2006020102), National Natural Science Foundation of China (grants. 41971092, 41961134035, 41771085 and 41801034), the “Key Research Programs in Frontier Sciences” of the Chinese Academy of Sciences (grant QYZDY-SSW-DQC003), the National

Science Foundation Paleo Perspectives on Climate Change (Award 1502919) and National Key Research and Development Project (2019YFC1509102). We appreciate the anonymous reviewers for their insightful and constructive comments.

Declaration

Conflict of interest The authors declare that they have no conflict of interest.

References

- Aizen VB, Aizen EM, Melack JM, Kreutz KJ, Cecil LD (2004) Association between atmospheric circulation patterns and firn-ice core records from the Inilchek glacierized area, central Tien Shan, Asia. *J Geophys Res Atmos*. <https://doi.org/10.1029/2003JD003894>
- Anderson B, Mackintosh A (2012) Controls on mass balance sensitivity of maritime glaciers in the Southern Alps, New Zealand: the role of debris cover. *J Geophys Res Earth*. <https://doi.org/10.1029/2011JF002064>
- Armstrong RL et al (2019) Runoff from glacier ice and seasonal snow in High Asia: separating melt water sources in river flow. *Reg Environ Change* 19(5):1249–1261. <https://doi.org/10.1007/s10113-018-1429-0>
- Azam MF, Srivastava S (2020) Mass balance and runoff modelling of partially debris-covered Dokriani Glacier in monsoon-dominated Himalaya using ERA5 data since 1979. *J Hydrol* 590:125432. <https://doi.org/10.1016/j.jhydrol.2020.125432>
- Barandun M, Huss M, Sold L, Farinotti D, Azisov E, Salzmann N, Usabaliyev R, Merkushkin A, Hoelzle M (2015) Re-analysis of seasonal mass balance at Abramov glacier 1968–2014. *J Glaciol* 61(230):1103–1117. <https://doi.org/10.3189/2015JoG14J239>
- Bhattacharya A, Bolch T, Mukherjee K, King O, Menounos B, Kapitsa V, Neckel N, Yang W, Yao T (2021) High Mountain Asian glacier response to climate revealed by multi-temporal satellite observations since the 1960s. *Nat Commun* 12:4133. <https://doi.org/10.1038/s41467-021-24180-y>
- Bolch T, Yao T, Kang S, Buchroithner MF, Scherer D, Maussion F, Huintjes E, Schneider C (2010) A glacier inventory for the western Nyainqentanglha Range and the Nam Co Basin, Tibet, and glacier changes 1976–2009. *Cryosphere* 4(3):419–433. <https://doi.org/10.5194/tc-4-419-2010>
- Bonekamp PNJ, de Kok RJ, Collier E, Immerzeel WW (2019) Contrasting meteorological drivers of the glacier mass balance between the Karakoram and Central Himalaya. *Front Earth Sci* 7:107. <https://doi.org/10.3389/feart.2019.00107>
- Bothe O, Fraedrich K, Zhu X (2011) Large-scale circulations and Tibetan Plateau summer drought and wetness in a high-resolution climate model. *Int J Climatol* 31:832–846. <https://doi.org/10.1002/joc.2124>
- Brun F, Berthier E, Wagnon P, Kääb A, Treichler D (2017) A spatially resolved estimate of High Mountain Asia glacier mass balances from 2000 to 2016. *Nat Geosci* 10:668–673. <https://doi.org/10.1038/ngeo2999>
- Brun F, Wagnon P, Berthier E, Jomelli V, Maharjan SB, Shrestha F, Kraaijenbrink PDA (2019) Heterogeneous influence of glacier morphology on the mass balance variability in High Mountain Asia. *J Geophys Res Earth* 124(6):1331–1345. <https://doi.org/10.1029/2018JF004838>
- Brunt D (1932) Notes on radiation in the atmosphere. *Q J R Meteor Soc* 58:389–420. <https://doi.org/10.1002/qj.49705824704>
- Cao B, Pan B, Guan W, Wang J, Wen Z (2017) Changes in ice volume of the Ningchan No. 1 Glacier, China, from 1972 to 2014, as derived from in situ measurements. *J Glaciol* 63:1025–1033. <https://doi.org/10.1017/jog.2017.70>
- Cao B, Pan B, Wen Z, Guan W, Li K (2019) Changes in glacier mass in the Lenglongling Mountains from 1972 to 2016 based on remote sensing data and modeling. *J Hydrol* 578:124010. <https://doi.org/10.1016/j.jhydrol.2019.124010>
- Chen J, Qin X, Kang S, Du W, Sun W, Liu Y (2020) Potential effect of black carbon on glacier mass balance during the past 55 years of Laohugou Glacier No. 12, Western Qilian Mountains. *J Earth Sci* 31:410–418. <https://doi.org/10.1007/s12583-019-1238-5>
- Crawford TM, Duchon CE (1999) An improved parameterization for estimating effective atmospheric emissivity for use in calculating daytime downwelling longwave radiation. *J Appl Meteor* 38:474–480. [https://doi.org/10.1175/1520-0450\(1999\)038%3c0474:AIPFEE%3e2.0.CO;2](https://doi.org/10.1175/1520-0450(1999)038%3c0474:AIPFEE%3e2.0.CO;2)
- Ding Q, Wang B (2005) Circumglobal teleconnection in the Northern Hemisphere summer. *J Clim* 18:3483–3505. <https://doi.org/10.1175/JCLI3473.1>
- Ding B, Yang K, Yang W, He X, Chen Y, Lazhu GX, Wang L, Wu H, Yao T (2017) Development of a Water and Enthalpy Budget-based Glacier mass balance Model (WEB-GM) and its preliminary validation. *Water Resour Res* 53(4):3146–3178. <https://doi.org/10.1002/2016WR018865>
- Ding T, Yuan Y, Zhang J, Gao H (2019) 2018: the hottest summer in China and possible causes. *J Meteorol Res* 33:577–592. <https://doi.org/10.1007/s13351-019-8178-y>
- Farinotti D, Immerzeel WW, de Kok RJ, Quincey DJ, Dehecq A (2020) Manifestations and mechanisms of the Karakoram glacier Anomaly. *Nat Geosci* 13:8–16. <https://doi.org/10.1038/s41561-019-0513-5>
- Favier V, Wagnon P, Ribstein P (2004a) Glaciers of the outer and inner tropics: a different behaviour but a common response to climatic forcing. *Geophys Res Lett*. <https://doi.org/10.1029/2004GL020654>
- Favier V, Wagnon P, Chazarin J-P, Maisincho L, Coudrain A (2004b) One-year measurements of surface heat budget on the ablation zone of Antizana Glacier 15, Ecuadorian Andes. *J Geophys Res*. <https://doi.org/10.1029/2003jd004359>
- Fujita K, Ageta Y (2000) Effect of summer accumulation on glacier mass balance on the Tibetan Plateau revealed by mass-balance model. *J Glaciol* 46:244–252. <https://doi.org/10.3189/172756500781832945>
- Fujita K, Nuimura T (2011) Spatially heterogeneous wastage of Himalayan glaciers. *Proc Natl Acad Sci USA* 108(34):14011–14014. <https://doi.org/10.1073/pnas.1106242108>
- Fujita K, Sakai A (2014) Modelling runoff from a Himalayan debris-covered glacier. *Hydrol Earth Syst Sci* 18:2679–2694. <https://doi.org/10.5194/hess-18-2679-2014>
- Gao H, Feng Z, Zhang T, Wang Y, He X, Li H, Ren Z, Chen X, Zhang W, Duan Z (2021) Assessing glacier retreat and its impact on water resources in a headwater of Yangtze River based on CMIP6 projections. *Sci Total Environ* 765:142774. <https://doi.org/10.1016/j.scitotenv.2020.142774>
- Guo S, Chen R, Han C, Liu J, Wang X, Liu G (2021) Five-year analysis of evaporesublimation characteristics and its role on surface energy balance SEB on a Midlatitude Continental Glacier. *Earth Space Sci* 8(12):e2021EA001901. <https://doi.org/10.1029/2021ea001901>
- He J, Wang N, Chen A, Yang X, Hua T (2019) Glacier changes in the Qilian Mountains, Northwest China, between the 1960s and 2015. *Water* 11:623. <https://doi.org/10.3390/w11030623>
- Hock R, Holmgren B (2005) A distributed surface energy–balance model for complex topography and its application to

- Storglaciaren, Sweden. *J Glaciol* 51:25–36. <https://doi.org/10.3189/172756505781829566>
- Hoffman MJ, Fountain AG, Liston GE (2008) Surface energy balance and melt thresholds over 11 years at Taylor Glacier, Antarctica. *J Geophys Res Earth* 113(F4):F04014. <https://doi.org/10.1029/2008JF001029>
- Hoffman MJ, Fountain AG, Liston GE (2014) Near-surface internal melting: a substantial mass loss on Antarctic Dry Valley glaciers. *J Glaciol* 60(220):361–374. <https://doi.org/10.3189/2014JG13J095>
- Immerzeel WW et al (2020) Importance and vulnerability of the world's watertowers. *Nature* 577:364–369. <https://doi.org/10.1038/s41586-019-1822-y>
- Jiang X, Wang N, He J, Wu X, Song G (2010) A distributed surface energy and mass balance model and its application to a mountain glacier in China. *Chin Sci Bull* 55:2079–2087. <https://doi.org/10.1007/s11434-010-3068-9>
- Kääb A, Treichler D, Nuth C, Berthier E (2015) Brief Communication: contending estimates of 2003–2008 glacier mass balance over the Pamir–Karakoram–Himalaya. *Cryosphere* 9(2):557–564. <https://doi.org/10.5194/tc-9-557-2015>
- Kääb A et al (2018) Massive collapse of two glaciers in western Tibet in 2016 after surge-like instability. *Nat Geosci* 12:114–120. <https://doi.org/10.1038/s41561-017-0039-7>
- Kang S, Zhang Y, Qian Y, Wang H (2020) A review of black carbon in snow and ice and its impact on the cryosphere. *Earth Sci Rev* 210:103346. <https://doi.org/10.1016/j.earscirev.2020.103346>
- Kobayashi S et al (2015) The JRA–55 Reanalysis: General specifications and basic characteristics. *J Meteor Soc Jpn* 93:5–48. <https://doi.org/10.2151/jmsj.2015-001>
- Kumar P, Saharwardi MS, Banerjee A, Azam MFA, Dubey AK, Murtugudde R (2019) Snowfall variability dictates glacier mass balance variability in Himalaya–Karakoram. *Sci Rep* 9:18192. <https://doi.org/10.1038/s41598-019-54553-9>
- Li J, Ruan CQ (2018) The North Atlantic–Eurasian teleconnection in summer and its effects on Eurasian climates. *Environ Res Lett* 13:024007. <https://doi.org/10.1088/1748-9326/aa9d33>
- Li Z, Gao Y, Wang Y, Pan Y, Li J, Chen A, Wang T, Han C, Song Y, Theakstone WH (2015) Can monsoon moisture arrive in the Qilian Mountains in summer? *Quat Int* 358:113–125. <https://doi.org/10.1016/j.quaint.2014.08.046>
- Li J, Wang Y, Li J (2019a) Glacier outlines over the Qilian Mountain area (1980–2015). National Tibetan Plateau Data Center. <https://doi.org/10.11888/Geogra.tpdc.270234>
- Li J, Zheng F, Sun C, Feng J, Wang J (2019b) Pathways of influence of the Northern Hemisphere mid-high latitudes on East Asian climate: a review. *Adv Atmos Sci* 36(9):902–921. <https://doi.org/10.1007/s00376-019-8236-5>
- Liu Y (2018) Dataset of mass balance on the Laohugou Glacier No. 12, western Qi-lian Mountains (2014–2018). National Tibetan Plateau Data Center. <https://doi.org/10.11888/Glacio.tpdc.270006>
- Liu Q, Liu S (2016) Response of glacier mass balance to climate change in the Tianshan Mountains during the second half of the twentieth century. *Clim Dyn* 46(1):303–316. <https://doi.org/10.1007/s00382-015-2585-2>
- Liu W, Zhang D, Qin X, van den Broeke MR, Jiang Y, Yang D, Ding M (2021) Monsoon Clouds Control the Summer Surface Energy Balance on East Rongbuk Glacier (6,523 m Above Sea Level) the Northern of Mt. Qomolangma (Everest). *J Geophys Res Atmos* 126(8):e2020JD033998. <https://doi.org/10.1029/2020JD033998>
- Marzeion B, Cogley JG, Richter K, Parkes D (2014) Attribution of global glacier mass loss to anthropogenic and natural causes. *Science* 345(6199):919–921. <https://doi.org/10.1126/science.1254702>
- Mattea E, Machguth H, Kronenberg M, van Pelt W, Bassi M, Hoelzle M (2021) Firn changes at Colle Gnifetti revealed with a high-resolution process-based physical model approach. *Cryosphere* 15:3181–3205. <https://doi.org/10.5194/tc-15-3181-2021>
- Maurer JM, Schaefer JM, Rupper S, Corley A (2019) Acceleration of ice loss across the Himalayas over the past 40 years. *Sci Adv* 5(6):eaav7266. <https://doi.org/10.1126/sciadv.aav7266>
- Mölg T, Maussion F, Scherer D (2014) Mid-latitude westerlies as a driver of glacier variability in monsoonal High Asia. *Nat Clim Change* 4:68–73. <https://doi.org/10.1038/nclimate2055>
- Mölg T, Maussion F, Collier E, Chiang JC, Scherer D (2017) Prominent midlatitude circulation signature in High Asia's surface climate during monsoon. *J Geophys Res Atmos* 122(23):12702–12712. <https://doi.org/10.1002/2017JD027414>
- Möller M, Obleitner F, Reijmer CH, Pohjola VA, Głowacki P, Kohler J (2016) Adjustment of regional climate model output for modeling the climatic mass balance of all glaciers on Svalbard. *J Geophys Res Atmos* 121:5411–5429. <https://doi.org/10.1002/2015JD024380>
- Neckel N, Kropáček J, Bolch T, Hochschild V (2014) Glacier mass changes on the Tibetan Plateau 2003–2009 derived from ICESat laser altimetry measurements. *Environ Res Lett* 9(1):014009. <https://doi.org/10.1088/1748-9326/9/1/014009>
- Nie Y, Pritchard HD, Liu Q, Hennig T, Wang W, Wang X, Liu S, Nepal S, Samyn D, Hewitt D, Chen X (2021) Glacial change and hydrological implications in the Himalaya and Karakoram. *Nat Rev Earth Environ* 2(2):91–106. <https://doi.org/10.1038/s43017-020-00124-w>
- Oerlemans J (2001) *Glaciers and climate change*. AA Balkema Publishers, Rotterdam
- Oerlemans J, Knap W (1998) A 1 year record of global radiation and albedo in the ablation zone of Morteratschgletscher, Switzerland. *J Glaciol* 44:231–238. <https://doi.org/10.3189/S002214300002574>
- Oerlemans J et al (1998) Modelling the response of glaciers to climate warming. *Clim Dyn* 14(4):267–274. <https://doi.org/10.1007/s003820050222>
- Ohmura A (2001) Physical basis for the temperature-based melt-index method. *J Appl Meteorol* 40:753–761. [https://doi.org/10.1175/1520-0450\(2001\)040%3c0753:PBFTTB%3e2.0.CO;2](https://doi.org/10.1175/1520-0450(2001)040%3c0753:PBFTTB%3e2.0.CO;2)
- Pan B, Cao B, Wang J, Zhang G, Zhang C, Hu Z, Huang B (2012) Glacier variations in response to climate change from 1972 to 2007 in the western Lenglongling mountains, northeastern Tibetan Plateau. *J Glaciol* 58:879–888. <https://doi.org/10.3189/2012JoG12J032>
- Pritchard HD (2019) Asia's shrinking glaciers protect large populations from drought stress. *Nature* 569:649–654. <https://doi.org/10.1038/s41586-019-1240-1>
- Pu J, Yao T, Duan K, Sakai A, Fujita K, Matsuda Y (2005) Mass balance of the Qiyi glacier in the Qilian mountains: a new observation. *J Glaciol Geocryol* 27(2):199–206 (in Chinese)
- Qin X (2018) Daily value dataset of 10m meteorological tower at Laohugou Glacier No.12 in the Qilian Mountains of China (V1.0). National Tibetan Plateau Data Center. <https://doi.org/10.11888/Glacio.tpdc.270004>
- Radić V, Bliss A, Beedlow AC, Hock R, Miles E, Cogley JG (2014) Regional and global projections of twenty-first century glacier mass changes in response to climate scenarios from global climate models. *Clim Dyn* 42(1–2):37–58. <https://doi.org/10.1007/s00382-013-1719-7>
- Rayner NA, Parker DE, Horton EB, Folland CK, Alexander LV, Rowell DP, Kent EC, Kaplan A (2003) Global analyses of sea surface temperature, sea ice, and night marine air temperature since the

- late nineteenth century. *J Geophys Res Atmos*. <https://doi.org/10.1029/2002JD002670>
- Reijmer CH, Hock R (2008) Internal accumulation on Storglaciären, Sweden, in a multi-layer snow model coupled to a distributed energy- and mass balance model. *J Glaciol* 54(184):61–72. <https://doi.org/10.3189/002214308784409161>
- Saeed S, Miiller WA, Hagemann S, Jacob D (2011) Circumglobal wave train and the summer monsoon over northwestern India and Pakistan: the explicit role of the surface heat low. *Clim Dyn* 37:1045–1060. <https://doi.org/10.1007/s00382-010-0888-x>
- Sakai A, Matsuda Y, Fujita K, Matoba S, Uetake J, Satow K, Duan K, Pu J, Nakawo M, Yao T (2006) Meteorological observation at July 1st Glacier in northwest China from 2002 to 2005. *Bull Glacier Res* 23:23–32
- Sakai A, Nuimura T, Fujita K, Takenaka S, Nagai H, Lamsal D (2015) Climate regime of Asian glaciers revealed by GAMDAM glacier inventory. *Cryosphere* 9(3):865–880. <https://doi.org/10.5194/tc-9-865-2015>
- Shangguan D, Liu S, Ding Y, Wu L, Deng W, Guo W, Wang Y, Xu J, Yao X, Guo Z, Zhu W (2014) Glacier changes in the Koshi River basin, central Himalaya, from 1976 to 2009, derived from remote-sensing imagery. *Ann Glaciol* 55(66):61–68. <https://doi.org/10.3189/2014AoG66A057>
- Shean DE, Bhushan S, Montesano P, Rounce DR, Arendt A, Osmanoglu B (2020) A systematic, regional assessment of High Mountain Asia Glacier mass balance. *Front Earth Sci* 7:363. <https://doi.org/10.3389/feart.2019.00363>
- Shi Y, Liu S (2000) Estimation on the response of glaciers in China to the global warming in the 21st century. *Chin Sci Bull* 45:668–672. <https://doi.org/10.1007/BF02886048>
- Sicart JE, Wagnon P, Ribstein P (2005) Atmospheric controls of the heat balance of Zongo Glacier (16 S, Bolivia). *J Geophys Res Atmos*. <https://doi.org/10.1029/2004JD005732>
- Sun W, Qin X, Xu Y, Wu X, Liu Y, Ren J (2011) Annual variations of the components of radiation on the Laohugou No. 12 Glacier in the Qilian Mountains. *Adv Earth Sci* 26:347–352 (in Chinese)
- Sun M, Liu S, Yao X, Guo W, Xu J (2018a) Glacier changes in the Qilian Mountains in the past half-century: Based on the revised First and Second Chinese Glacier Inventory. *J Geograph Sci* 28:206–220. <https://doi.org/10.1007/s11442-018-1468-y>
- Sun W, Qin X, Wang Y, Chen J, Du W, Zhang T, Huai B (2018b) The response of surface mass and energy balance of a continental glacier to climate variability, western Qilian Mountains. *China Clim Dyn* 50(9):3557–3570. <https://doi.org/10.1007/s00382-017-3823-6>
- Thompson LG (2000) Ice core evidence for climate change in the Tropics: implications for our future. *Quaternary Sci Rev* 19:19–35. [https://doi.org/10.1016/S0277-3791\(99\)00052-9](https://doi.org/10.1016/S0277-3791(99)00052-9)
- Thompson LG, Mosley-Thompson E, Davis ME, Bolzan JF, Dai J, Klein L, Yao T, Wu X, Xie Z, Gundestrup N (1989) Holocene-late Pleistocene climatic ice core records from Qinghai-Tibetan Plateau. *Science* 246:474–477. <https://doi.org/10.1126/science.246.4929.474>
- Van Pelt W et al (2019) A long-term dataset of climatic mass balance, snow conditions, and runoff in Svalbard (1957–2018). *Cryosphere* 13:2259–2280. <https://doi.org/10.5194/tc-13-2259-2019>
- Vandecrux B, Colgan W, Solgaard AM, Steffensen JP, Karlsson NB (2021) Firn evolution at camp century, Greenland: 1966–2100. *Front Earth Sci*. <https://doi.org/10.3389/feart.2021.578978>
- Vuille M, Kaser G, Juen I (2008) Glacier mass balance variability in the Cordillera Blanca, Peru and its relationship with climate and the large-scale circulation. *Glob Planet Change* 62(1):14–28. <https://doi.org/10.1016/j.gloplacha.2007.11.003>
- Wagnon P et al (2013) Seasonal and annual mass balances of Mera and Pokalde glaciers (Nepal Himalaya) since 2007. *Cryosphere* 7:1769–1786. <https://doi.org/10.5194/tc-7-1769-2013>
- Wang N, He J, Jiang X, Song G, Wu X, Chen L (2009) Study on the zone of maximum precipitation in the north slopes of the central Qilian Mountains. *J Glaciol Geocryol* 31:395–403 (in Chinese)
- Wang N, He J, Pu J, Jiang X, Jing Z (2010) Variations in equilibrium line altitude of the Qiyi Glacier, Qilian Mountains, over the past 50 years. *Chin Sci Bull* 55:3810–3817. <https://doi.org/10.1007/s11434-010-4167-3>
- Wang S, Yao T, Tian L, Pu J (2017) Glacier mass variation and its effect on surface runoff in the Beida River catchment during 1957–2013. *J Glaciol* 63:523–534. <https://doi.org/10.1017/jog.2017.13>
- Wu J, Gao X (2013) A gridded daily observation dataset over China region and comparison with the other datasets. *Chin J Geophys* 56:1102–1111. <https://doi.org/10.6038/cjg20130406> (In Chinese)
- Xu Y, Gao X, Shen Y, Xu C, Shi Y, Giorgi A (2009) A daily temperature dataset over China and its application in validating a RCM simulation. *Adv Atmos Sci* 26:763–772. <https://doi.org/10.1007/s00376-009-9029-z>
- Yang K, Huang G, Tamai N (2001) A hybrid model for estimating global solar radiation. *Sol Energy* 70:13–22. [https://doi.org/10.1016/S0038-092X\(00\)00121-3](https://doi.org/10.1016/S0038-092X(00)00121-3)
- Yang W, Guo X, Yao T, Yang K, Zhao L, Li S, Zhu M (2011) Summer-time surface energy budget and ablation modeling in the ablation zone of a maritime Tibetan glacier. *J Geophys Res Atmos*. <https://doi.org/10.1029/2010JD015183>
- Yang W, Yao T, Guo X, Zhu M, Li S, Kattel DB (2013) Mass balance of a maritime glacier on the southeast Tibetan Plateau and its climatic sensitivity. *J Geophys Res Atmos* 118:9579–9594. <https://doi.org/10.1002/jgrd.50760>
- Yang K, Wu H, Qin J, Lin C, Tang W, Chen Y (2014) Recent climate changes over the Tibetan Plateau and their impacts on energy and water cycle: a review. *Global Planet Change* 112:79–91. <https://doi.org/10.1016/j.gloplacha.2013.12.001>
- Yang W, Guo X, Yao T, Zhu M, Wang Y (2016) Recent accelerating mass loss of southeast Tibetan glaciers and the relationship with changes in macroscale atmospheric circulations. *Clim Dyn* 47:805–815. <https://doi.org/10.1007/s00382-015-2872-y>
- Yao T, Li Z, Thompson LG, Thompson EM, Wang Y, Tian L, Wang N, Duan K (2006) $\delta^{18}\text{O}$ records from Tibetan ice cores reveal differences in climatic changes. *Ann Glaciol* 43(1):1–7. <https://doi.org/10.3189/172756406781812131>
- Yao T, Thompson L, Yang W, Yu W, Gao Y, Guo X, Yang X, Duan K, Zhao H, Xu B (2012) Different glacier status with atmospheric circulations in Tibetan Plateau and surroundings. *Nat Clim Change* 2:663–667. <https://doi.org/10.1038/nclimate1580>
- Yao T, Masson-Delmotte V, Gao J, Yu W, Yang X, Risi C, Sturm C, Werner M, Zhao H, He Y, Ren W, Tian L, Shi C, Hou S (2013) A review of climatic controls on $\delta^{18}\text{O}$ in precipitation over the Tibetan Plateau: observations and simulations. *Rev Geophys* 51(4):525–548. <https://doi.org/10.1002/rog.20023>
- Yao T, Xue Y, Chen D, Chen F, Thompson LG, Cui P, Koike T, Lau WKM, Lettenmaier D, Mosbrugger V (2019) Recent third pole's rapid warming accompanies cryospheric melt and water cycle intensification and interactions between monsoon and environment: multidisciplinary approach with observations, modeling, and analysis. *Bull Am Meteorol Soc* 100:423–444. <https://doi.org/10.1175/BAMS-D-17-0057.1>
- Ye Q, Zong J, Tian L, Cogley JG, Song C, Guo W (2017) Glacier changes on the Tibetan Plateau derived from Landsat imagery: mid-1970s–2000–13. *J Glaciol* 63(238):273–287. <https://doi.org/10.1017/jog.2016.137>
- Yuan Q, Wu S, Zhao D, Dai E, Yuan Q, Ren P (2021) Regional differences in surface air temperature changing patterns from 1960 to 2016 of China. *Clim Dyn* 57(7):1733–1749. <https://doi.org/10.1007/s00382-021-05774-0>

- Zemp M et al (2019) Global glacier mass changes and their contributions to sea-level rise from 1961 to 2016. *Nature* 568(7752):382–386. <https://doi.org/10.1038/s41586-019-1071-0>
- Zhang Y, Hirabayashi Y, Liu S (2012) Catchment-scale reconstruction of glacier mass balance using observations and global climate data: Case study of the Hailuoguo catchment, southeastern Tibetan Plateau. *J Hydrol* 444:146–160. <https://doi.org/10.1016/j.jhydrol.2012.04.014>
- Zhang Y, Enomoto H, Ohata T, Kitabata H, Kadota T, Hirabayashi Y (2016) Projections of glacier change in the Altai Mountains under twenty-first century climate scenarios. *Clim Dyn* 47(9):2935–2953. <https://doi.org/10.1007/s00382-016-3006-x>
- Zhang H, Li Z, Zhou P (2021) Mass balance reconstruction for Shiyi Glacier in the Qilian Mountains, Northeastern Tibetan Plateau, and its climatic drivers. *Clim Dyn* 56:969–984. <https://doi.org/10.1007/s00382-020-05514-w>
- Zhao C, Zhang R (2019) Qilian Mountains integrated observatory network: cold and arid research network of Lanzhou university (an observation system of meteorological elements gradient of Xiyinghe station, 2018). National Tibetan Plateau Data Center. <https://doi.org/10.11888/Geogra.tpcd.270158>. CSTR: 18046.11. Geogra.tpcd.270158
- Zhou Y, Li Z, Li J, Zhao R, Ding X (2018) Glacier mass balance in the Qinghai-Tibet Plateau and its surroundings from the mid-1970s to 2000 based on Hexagon KH-9 and SRTM DEMs. *Remote Sens Environ* 210:96–112. <https://doi.org/10.1016/j.rse.2018.03.020>
- Zhou C, Zhao P, Chen J (2019) The interdecadal change of summer water vapor over the Tibetan Plateau and associated mechanisms. *J Clim* 32:4103–4119. <https://doi.org/10.1175/JCLI-D-18-0364.1>
- Zhu L, Peng P (2019) Meteorological data of surface environment and observation network in China's cold region (2014–2017). National Tibetan Plateau Data Center. <https://doi.org/10.11888/Geogra.tpcd.270280>
- Zhu M, Yao T, Yang W, Xu B, Wang X (2017) Evaluation of parameterizations of incoming longwave radiation in the highmountain region of the Tibetan Plateau. *J Appl Meteorol Clim* 56(4):833–848. <https://doi.org/10.1175/JAMC-D-16-0189.1>
- Zhu M, Yao T, Yang W, Xu B, Wu G, Wang X (2018a) Differences in mass balance behavior for three glaciers from different climatic regions on the Tibetan Plateau. *Clim Dyn* 50:3457–3484. <https://doi.org/10.1007/s00382-017-3817-4>
- Zhu M, Yao T, Yang W, Xu B, Wu G, Wang X, Xie Y (2018b) Reconstruction of the mass balance of Muztag Ata No. 15 glacier, eastern Pamir, and its climatic drivers. *J Glaciol* 64:259–274. <https://doi.org/10.1017/jog.2018.16>
- Zhu M, Yao T, Xie Y, Xu B, Yang W, Yang S (2020) Mass balance of Muji Glacier, northeastern Pamir, and its controlling climate factors. *J Hydrol* 590:125447. <https://doi.org/10.1016/j.jhydrol.2020.125447>
- Zhu M, Yang W, Yao T, Tian L, Thompson LG, Zhao H (2021a) The influence of key climate variables on mass balance of Naimona'nyi Glacier on a north-facing slope in the western Himalayas. *J Geophys Res Atmos* 126(7):e2020JD033956. <https://doi.org/10.1029/2020JD033956>
- Zhu M, Thompson LG, Zhao H, Yao T, Yang W, Jin S (2021b) Influence of atmospheric circulation on glacier mass balance in western Tibet: an analysis based on observations and modeling. *J Clim* 34(16):6743–6757. <https://doi.org/10.1175/JCLI-D-20-0988.1>

Publisher's Note Springer Nature remains neutral with regard to jurisdictional claims in published maps and institutional affiliations.